Energy and AI 3 (2021) 100047

Contents lists available at ScienceDirect

Energy and AI

journal homepage: www.elsevier.com/locate/egyai

Lévy-flight moth-flame optimisation algorithm-based micro-grid equipment sizing: An integrated investment and operational planning approach

Soheil Mohseni [a,*], Alan C. Brent [a,b], Daniel Burmester [a], Will N. Browne [a]

[a] Sustainable Energy Systems, Faculty of Engineering, Victoria University of Wellington, Wellington 6140, New Zealand
[b] Department of Industrial Engineering and the Centre for Renewable and Sustainable Energy Studies, Stellenbosch University, Stellenbosch 7600, South Africa

HIGHLIGHTS

- A Lévy-flight moth-flame optimisation algorithm-based micro-grid (MG) sizing model is proposed.
- A day-ahead operational planning optimisation framework is nested within the optimal sizing model.
- The superiority of the Lévy-flight moth-flame optimiser to a range of well-established meta-heuristics is shown.
- The effectiveness of the model is demonstrated by benchmarking it against the HOMER Pro software.
- The profitability is improved by at least 18% for a community MG scheme in rural New Zealand.

GRAPHICAL ABSTRACT

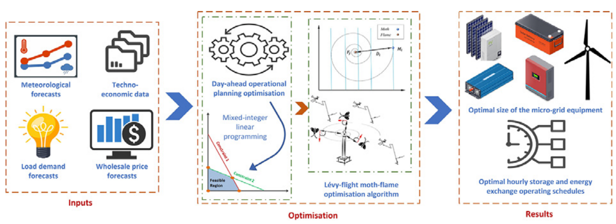

ARTICLE INFO

Article history:
Received 13 December 2020
Received in revised form 13 January 2021
Accepted 14 January 2021
Available online 20 January 2021

Keywords:
Micro-grid
Techno-economic
Meta-heuristic
Optimal sizing
Operational planning
Smart grid
Optimization

ABSTRACT

Bridging the gap between simulation and reality for successful micro-grid (MG) implementation requires accurate mathematical modelling of the underlying energy infrastructure and extensive optimisation of the design space defined by all possible combinations of the size of the equipment. While exact mathematical optimisation approaches to the MG capacity planning are highly computationally efficient, they often fail to preserve the associated problem nonlinearities and non-convexities. This translates into the fact that the available MG sizing tools potentially return a sub-optimal (inferior) MG design. This brings to light the importance of nature-inspired, swarm-based meta-heuristic optimisation algorithms that are able to effectively handle the nonlinear and non-convex nature of the MG design optimisation problem – and better approximate the globally optimum solution – though at the expense of increased computational complexity. Accordingly, this paper introduces a robust MG capacity planning optimisation framework based on a state-of-the-art meta-heuristic, namely the Lévy-flight moth-flame optimisation algorithm (MFOA). An intelligent linear programming-based day-ahead energy scheduling design is, additionally, integrated into the proposed model. A case study is presented for a real grid-tied community MG in rural New Zealand. A comparison of the modelling results with those of the most popular tool in the literature and industry, HOMER Pro, verifies the superiority of the proposed meta-heuristic-based MG sizing model. Additionally, the efficiency of the Lévy-flight MFOA is compared to nine well-established meta-heuristics in the MG capacity planning literature. The comparative analyses have revealed the statistically significant outperformance of the Lévy-flight MFOA to the examined meta-heuristics. Notably, its superiority to the original MFOA, the hybrid genetic algorithm-particle swarm optimisation, and the ant colony optimiser, by at least ~6.5%, ~8.4%, and ~12.8%, is demonstrated. Moreover, comprehensive capital budgeting analyses have confirmed the financial viability of the test-case system optimised by the proposed model.

* Corresponding author.
E-mail address: soheil.mohseni@ecs.vuw.ac.nz (S. Mohseni).

https://doi.org/10.1016/j.egyai.2021.100047

Nomenclature

CC	capital cost
CL	component lifetime
CRF	capital recovery factor
$C_{B,r}$	rated capacity of each battery pack
$C_{tr,n}$	total cost of energy exchanges with the grid
D	cycle-life degradation factor of the battery
DOD	depth of discharge
D_{ij}	distance between moth i and flame j
$E_B(t)$	energy content of the battery bank in time t
F_j	j-th flame
$I_G(t)$	global horizontal irradiance in time t
$LCOE$	levelised cost of energy
$LPSP$	loss of power supply probability
$LPSP^{max}$	maximum allowed loss of power supply probability
M_i	i-th moth
$NOCT$	nominal operating cell temperature
$NPC_{tr,net}$	net present cost of power exchanged with the grid
NPC_c	net present cost of component c
N_c	optimal size of component c
N_c^{max}	maximum allowed size of component c
$O\&M$	operation and maintenance cost
$OPEX$	operating expenditure
PL	project lifetime
$P_{WT,r}$	rated power of wind turbines
P_c^{min}, P_c^{max}	minimum/maximum allowed operating power of component c
$P_{ch,B}(t)$, $P_{dch,B}(t)$	charging/discharging power of the battery bank in time t
$P_{ch,B}^{max}$, $P_{dch,B}^{max}$	maximum charging/discharging power of the battery bank
$P_{ch,B}^{min}$, $P_{dch,B}^{min}$	minimum charging/discharging power of the battery bank
$P_{im}(t)$, $P_{ex}(t)$	grid import/export power in time t
P_L	power load
P_{PV}	power output from photovoltaic plant
P_{WT}	power output from wind plant
$P_c(t)$	operating power of component c in time t
$\dot{Q}$	losses in the series resistance of the battery
RC	replacement cost
$SPPW$	single-payment present-worth factor
SSR	self-sufficiency ratio
SSR^{min}	minimum allowed self-sufficiency ratio
SV	salvage value
$T_{c,ref}$	reference solar cell temperature
$T_a(t)$	ambient temperature in time t
$T_c(t)$	solar cell temperature in time t
$T_i(t)$	internal operating temperature of the battery in time t
T_i^{min}, T_i^{max}	minimum/maximum allowed internal operating temperature of the battery
WLC_{MG}	whole-life cost of the micro-grid
a_{PV}	area of each photovoltaic panel
c	specific heat capacity of the battery
$\eta_{ch,B}$, $\eta_{dch,B}$	battery charging/discharging efficiency
$\eta_{PV}(t)$	solar photovoltaic panel efficiency in time t
η_r	rated efficiency of photovoltaic panels
h	battery thermal conductance to ambient temperature
ir	real interest rate
kt	rate of increase of the calendar degradation factor of the battery
m	mass of the battery
p	penalty factor
$v(t)$	wind speed in time t
v_{ci}	cut-in wind speed
v_{co}	cut-out wind speed
v_r	rated wind speed
π	wholesale electricity market price
σ_B	battery self-discharge rate
Δt	duration of time-step

1. Introduction

The micro-grid (MG) infrastructure capacity planning optimisation involves determining the whole life cost-optimal mix of the sizes of the candidate distributed energy resources and conversion devices so as to meet the energy requirements at a prescribed reliability level subject to a set of operational and planning constraints [1–3].

1.1. Literature review

Several review studies have discussed approaches and trends for MG energy planning and capacity optimisation. Gamarra and Guerrero [4], Fathima and Palanisamy [5], as well as, more recently, Emad et al. [6] analyse the MG design optimisation literature; Sinha and Chandel [7], Hannan et al. [8], as well as Yang et al. [9], review the methods and algorithms for sizing energy storage systems; while Mellit and Kalogirou [10] discuss various artificial intelligence (AI) techniques used for the optimal sizing of photovoltaic (PV) systems. The optimisation approaches developed in the literature on the capacity planning of renewable and sustainable energy systems can be broadly categorised as either based on the exact mathematical optimisation algorithms or (AI) techniques, the most widely-used of which are summarised in Fig. 1.

Table 1 presents a summary of the notable studies in the optimal MG sizing literature that have provided closed-form solutions to the problem. The main issue associated with exact mathematical optimisation algorithms in the context of MG designing and sizing is that they require strong assumptions and implications to be made on the structure of the underlying objective function, such as convexity, linearity, continuity, differentiability, and so forth. This is because the optimal MG sizing problem has been shown to be associated with non-deterministic polynomial time-hardness (NP-hardness) [11,12]. This means that although formulating the economic MG energy planning problem such that it is amenable to exact mathematical solution algorithms considerably alleviates the computational burden, it substantially increases the risk of sub-optimality – or, in other words, it can result in a loss of solution fidelity, especially for highly nonlinear and non-convex design problems [13]. Associated developed simplified solution approaches, based on mathematical optimisation techniques, have included various decomposition techniques, linear programming (LP), mixed-integer programming (MIP), mixed-integer linear programming (MILP), mixed-integer nonlinear programming (MINLP), and dynamic programming, of which MILP is the most popular approach.

However, given that the optimal MG asset allocation is an off-line, one-time process, it can be argued that computational complexity should not be the primary concern from an optimisation point of view, provided that optimising a solution to the problem is not computationally intractable. In this light, a recent, emerging strand of the long-term MG investment planning literature has proposed using AI-based meta-heuristic optimisation algorithms as an alternative to classical optimisation methods. The MG energy planning optimisation literature has convincingly demonstrated that meta-heuristic optimisation algorithms

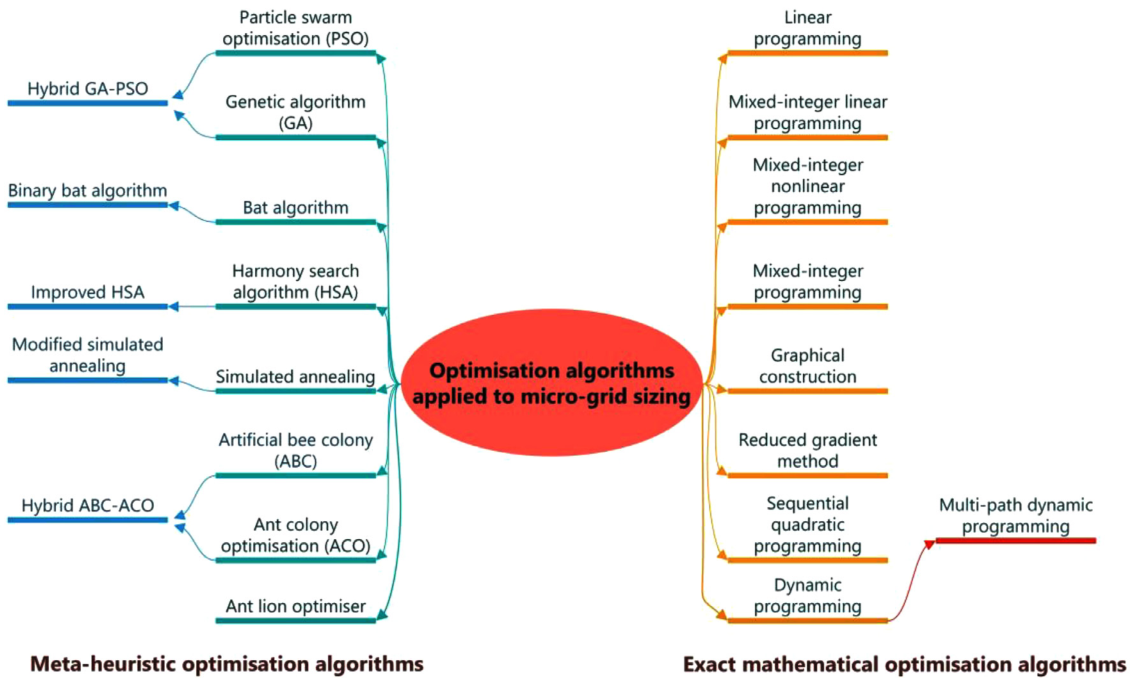

Fig. 1. Categorisation of the optimisation techniques applied to the MG capacity allocation problem.

Table 1
Summary of the notable studies employing exact mathematical optimisation algorithms for MG sizing.

Reference	System architecture	Optimisation method	Sizing variables	Bus (AC/DC)	Main objectives
[14]	An off-grid solar PV/battery MG	MILP	Solar PV panels, battery bank	DC	Economic
[15]	A combined heat and power (CHP) MG	MILP	CHP system	AC	Economic, reliability
[16]	A wind power plant/hydrogen energy storage system	Dynamic programming	Hydrogen tank	AC	Economic
[17]	A conventional power system	LP	Solar PV panels, wind turbines, fuel cells, micro-turbines	AC	Economic, reliability
[18]	An off-grid MG system	Lagrange multipliers	Distributed energy resources	DC	Economic
[19]	A stand-alone MG that consists of wind turbines, diesel generators, and a hydrogen system	MIP	Wind turbines, diesel generators, fuel cells, electrolyser, hydrogen tank	AC	Economic
[20]	A grid-tied MG that consists of solar PV panels, wind turbines, diesel generators, and a hydrogen system	MIP	Solar PV panels, wind turbines, diesel generators, fuel cells, electrolyser, hydrogen tank	DC	Economic
[21]	A grid-tied boiler/micro-CHP/heat storage system	MILP	Boiler, micro-CHP, heat storage	AC	Economic, greenhouse gas emissions

could be effectively used to optimise an efficient solution to the MG sizing problem [22–26]. The main advantage of meta-heuristics over exact mathematical approaches in this context is their ability to solve the NP-hard problem at hand in polynomial time, while effectively handling the model-inherent nonlinearities and non-convexities. Table 2 summarises the notable studies that have adopted a meta-heuristic-based MG sizing approach. The most widely-used meta-heuristic algorithms in the literature include: the particle swarm optimisation (PSO) [27], the genetic algorithm (GA) [28], the hybrid GA-PSO [29], the harmony search (HS) [30], the simulated annealing (SA) [31], the artificial bee colony (ABC) [32], the ant colony optimisation (ACO) [33], and the ant lion optimiser (ALO) [34].

In addition, a series of recent academic papers [53–55] have shown the statistical significance and superiority of the moth-flame optimisation algorithm (MFOA) [56] to more than 30 meta-heuristics (including well-established and state-of-the-art algorithms) when applied to different on- and off-grid MG configurations considering various technologies in the candidate pool.

Moreover, to support the stakeholder decision-making process on the cost-optimal mix of energy generation, storage, and conversion technologies, many MG design optimisation and long-term investment planning software tools exist in the literature and industry [57,58]. The solution approaches used in the available tools can be broadly classified into two groups.

The first class of the tools takes a simplistic full-factorial approach to solving the optimal design problem. The most notable software packages in this group are HOMER [59] and RETScreen [60]. Given that the full-factorial approach selects component sizes at a limited number of fixed intervals, it cannot be formally considered as an ‘optimal’ solution [61]. Furthermore, it leads to the ‘combinatorial explosion’ when increasing the granularity of the search space and/or increasing the number of candidate technologies above a low critical value.

The second, more algorithmically complex class of the existing tools employ a linearized approach to equipment capacity planning, such as MILP. The notable software packages in this group include: HOMER Pro [62], Hybrid2 [63], SAM [64], XENDEE [65], REOpt [66], and DER-CAM [67]). A simplified exact mathematical problem formulation is used in these tools by providing convex constraints. That is, these tools are plagued by the same significant deficiencies as exact mathematical optimisation-based solution algorithms.

Table 2
Summary of the notable studies employing meta-heuristic optimisation algorithms for MG sizing.

Reference	System architecture	Optimisation method(s)	Sizing variables	Bus (AC/DC)	Main objective(s)
[35]	An off-grid MG that consists of wind turbines, a waste-to-energy plant, and a hydrogen-based storage system	PSO	Wind turbines, converter, fuel cell, electrolyser, hydrogen tank	DC	Economic
[36]	A grid-connected MG that consists of solar PV panels, battery packs, and a hydrogen-based storage system	GA	PV panels, fuel cell, electrolyser, hydrogen tank, battery	DC	Economic
[37]	A stand-alone PV/wind/battery MG	HS	PV panels, wind turbines, battery bank	AC	Economic
[38]	An off-grid solar PV/wind turbine/battery MG	ACO	PV panels, wind turbines	AC	Economic
[39]	A stand-alone MG that consists of solar PV panels, wind turbines, and a hydrogen storage system	ABC	PV panels, wind turbines, fuel cell, electrolyser, hydrogen tank	DC	Economic, loss of power supply probability
[22]	A stand-alone MG that consists of solar PV panels, battery packs, and a hydrogen-based storage system	PSO, HS, SA, tabu search	PV panels, wind turbines, fuel cell, electrolyser, hydrogen tank, battery	DC	Economic
[40]	An islanded solar PV/wind turbine/battery MG	SA	PV panels, wind turbines	DC	Economic, reliability
[41]	Three stand-alone MGs with different combinations of solar PV panels, wind turbines, biomass power plants, flywheels, micro-hydro power plants, hydrogen system, batteries, super-capacitors	Sine-cosine algorithm, multi-verse optimiser, water evaporation optimisation, hybrid GA-PSO	PV panels, wind turbines, battery packs, electrolysers, fuel cells, hydrogen tanks, super-capacitors, biopower plants, micro-hydro plants, and flywheels	DC	Economic
[42]	A grid-tied solar PV/wind turbine/battery MG	PSO, GA, flower pollination algorithm	Battery bank	AC	Economic
[43]	An off-grid solar PV/wind turbine/tidal turbine/battery/diesel generator MG	Hybrid expert fuzzy system-grey wolf optimisation	Battery bank	DC	Economic
[44]	An off-grid solar PV/wind turbine/battery MG	Whale optimisation algorithm	Solar PV panels, wind turbines, battery packs, electric vehicle charging station, converters	DC	Economic
[45]	A non-grid-connected wind turbine/hydrogen/super-capacitor MG	Non-dominated sorting genetic algorithm II	Wind turbines, electrolyser, hydrogen tank, fuel cell, super-capacitor	DC	Economic, power quality
[46]	A grid-tied solar PV/wind turbine/fuel cell/hydrogen tank/boiler MG	Hybrid bird mating optimisation-differential evolution	Solar PV panels, wind turbines, fuel cell, hydrogen reservoir, boiler	DC	Economic
[47]	Three off-grid MGs with different combinations of solar PV panels, wind turbines, fuel cells, electrolysers, and hydrogen storage	Hybrid chaotic search-SA-HS	Solar PV panels, wind turbines, fuel cell, hydrogen tank, electrolyser	DC	Economic
[48]	An off-grid solar PV/wind turbine/electrolyser/hydrogen tank/fuel cell MG	Non-dominated sorting genetic algorithm II	Solar PV panels, wind turbines, fuel cell, hydrogen tank, electrolyser	DC	Economic, reliability, energy curtailment
[49]	An off-grid solar PV/wind turbine MG backed with different battery technologies	ALO, grey wolf optimiser, krill herd algorithm	Solar PV panels, wind turbines, and different battery technologies	DC	Economic
[50]	An off-grid solar PV/pumped hydro storage/battery bank/biogas generator MG for a radio transmitter station	Water cycle algorithm	Solar PV panels, pumped hydro storage, battery bank, biogas generator	DC	Economic
[51]	A grid-connected solar PV/wind turbine/battery bank/biomass gasifier MG	ABC, PSO	Solar PV panels, wind turbines, battery packs, and biomass gasifier	DC	Economic
[52]	An off-grid solar PV/wind turbine/battery MG	Multi-objective variants of the grasshopper optimisation, PSO, and cuckoo search optimisation algorithms	Solar PV panels, wind turbines, and battery packs	DC	Economic, reliability

1.2. Literature gaps

The above review of the long-term energy planning and MG design optimisation literature identifies crucial gaps in knowledge, giving rise to a set of specific research questions, namely:

- While the basic versions of meta-heuristics are continuously evolving, their improved variants are seldom applied to the optimal MG sizing problem. This raises the question to which extent meta-heuristic improvements actually matter in the context of MG planning. Accordingly, although its potential benefit in improving the population diversity and the efficiency of the local search process of the basic versions of meta-heuristics (around the global optima) has been demonstrated in a number of instances [68,69], Lévy-flight-supported meta-heuristics applied to MG capacity planning remain underutilised. In particular, a recently-improved variant of the MFOA, namely the Lévy-flight MFOA [70], has not yet been applied to the optimal MG capacity allocation problem.

- While many software packages tailored to the long-term MG investment planning problem are available in the literature and commercially, there is a capability gap in terms of estimating the globally-optimum solution, especially for large-scale systems and/or when seeking the cost-optimal sizes for a large number of technologies in the candidate pool. The research question following from this gap is how existing community-scale applicable software tools can be improved to more accurately calculate the optimal sizes of the MG components.
- An in-depth review of the meta-heuristic-based MG capacity planning approaches failed to identify any such models integrating an optimisation-based energy dispatch strategy. The reason lies in the time-consuming nature of the meta-heuristic-based solution algorithms, making them intractable to include any look-ahead scheduling provisions – that need to be repeated for each of the hundreds of their search agents. Hence, a research question arises how a computationally-tractable MG dispatch optimisation framework can be designed for longer periods of time (e.g., one year), so that it can be integrated into meta-heuristic-based MG sizing approaches without incurring prohibitive computational constraints.

1.3. Contributions of paper

To address the literature gaps this paper introduces a robust, deterministic, global-search MG capacity-planning algorithm. Founded on the principles of meta-heuristic optimisation, the proposed model is able to handle high levels of nonlinearity and non-convexity in the objective function – and can be applied to MGs of any size and any architecture. In particular, the key contributions of the paper are:

1 The performance of the novel Lévy-flight MFOA is evaluated in MG capacity planning applications. To this end, it is accommodated in a standard meta-heuristic-based MG sizing model that includes the total discounted system cost as a decision criterion and ensures a user-specified level of energy reliability, which is estimated based on the typical one-year (8,760 h) MG operation simulations.

2 By leveraging the power and speed of the Lévy-flight MFOA, which is additionally reinforced with an adaptive stopping criterion, the model provides a platform to optimise the operation of MGs over a moving 24-h horizon using a LP-based approach in a computationally-feasible way during the investment planning phase. The optimal day-ahead energy dispatch algorithm is for the first time accommodated into a meta-heuristic-based MG capacity planning model enabling it to cost-optimally respond to the dynamic nature of the model input data – load demand, meteorological, and wholesale electricity market price – based on forward-looking predictions.

1.4. Paper organisation

The remainder of the paper is organised as follows. Section 2 presents the proposed Lévy-flight MFOA-based MG sizing model. A test-case MG system is laid out in Section 3 and the model is populated for the case of a rural community in New Zealand. Section 4 presents the solution of the model and validates its efficacy through a direct comparison with the industry-leading MG sizing software, HOMER Pro, as well as the most efficient meta-heuristics reported in the literature. Finally, conclusions are made and areas for further work are discussed in Section 5.

2. Methodology

The following sections lay out the structure of the proposed meta-heuristic-based long-term MG investment planning and capacity optimisation model.

2.1. Planning-level objective function

The objective is to minimise the whole-life cost of the project, which consists of the lifetime costs of the components and the total cost of power trading with the utility grid (i.e., net electricity imports) over the MG life-cycle in present value, as follows:

$$\min WLC_{MG} = \sum_{c\in C} NPC_c + NPC_{tr,net} + p, \tag{1}$$

where NPC_c denotes the net present cost of the candidate technology c that is included in the model for consideration, $NPC_{tr,net}$ is the cost of total net energy purchased from the upstream grid in present value, while p penalizes the solutions that violate any of the imposed constraints.

The net present cost of a component in the context of MG design and development refers to the present value of all the costs associated with its new installation, replacement, as well as operation and maintenance (O&M) over the life-cycle of the project. The term “present value” in this context describes costs that have been discounted back to the baseline year, which accounts for the growth of inflation and the rise of interest rates. Mathematically, the net present cost of a component can be expressed by the following equation [71]:

$$NPC_c = N_c \times \left(CC + RC \times SPPW + \frac{O\&M}{CRF(ir, PL)} - SV \right), \tag{2}$$

where N_c denotes the optimal capacity/quantity of component c, CC and RC respectively represent the capital cost and replacement cost of the component, $SPPW$ stands for the single-payment present-worth factor, which is defined in Eq. (3) [35],[1] $O\&M$ indicates the operation and maintenance cost of the component, CRF stands for the capital recovery factor that is a function of the real interest rate, ir, and the projected service life of the project, PL, as expressed in Eq. (5) [35],[2] and SV is the salvage value of the component, which is expressed in Eq. (6) [72].[3] Any additional residual value, other than what is reflected in the equipment salvage value, is assumed to be counterbalanced by the costs associated with the equipment recycling or disposal.

$$SPPW = \sum_{n=1}^{N} \frac{1}{(1+ir)^{CL\times n}}, \tag{3}$$

where CL denotes the component lifetime and N can be determined by the following equation:

$$N = \begin{cases} \left\lceil \frac{PL}{CL} \right\rceil - 1 \; if \; PL \; mod \; CL = 0, \\ \left\lceil \frac{PL}{CL} \right\rceil \; otherwise, \end{cases} \tag{4}$$

$$CRF(ir, PL) = \frac{ir(1+ir)^{PL}}{(1+ir)^{PL} - 1}, \tag{5}$$

$$SV = RC \times \frac{CL - \left(PL - CL \times \left\lfloor \frac{PL}{CL} \right\rfloor \right)}{CL}. \tag{6}$$

In addition, to adjust the energy exchange cost components for the real interest rate, the net present cost of the net energy purchased from the utility grid over the MG life-cycle can be obtained as [73]:

$$NPC_{tr,net} = \sum_{n=1}^{PL} \frac{C_{tr,n}}{(1+ir)^n}, \tag{7}$$

[1] The single-payment present-worth factor calculates the unknown present value of a lump sum payment needed that returns a known future value given the interest rate.

[2] The capital recovery factor is used to calculate the present value of a series of equal annual cash flows as a ratio of a constant annuity to the present value of receiving that annuity.

[3] The salvage value, alternatively referred to as resale value, scrap value, and residual value, is the estimated value that is expected at the end of the useful life of a MG asset, which is used to calculate the asset's depreciation expense.

where $C_{tr,n}$ denotes the total cost associated with the total net energy purchased from the grid in year n of the MG operation.

2.2. Planning-level constraints

Several constraints need to be relaxed at the planning level, namely: (1) a maximum allowed unreliability constraint measured by the loss of power supply probability ($LPSP$) index (Eq. (8)) [74], which is set to be equal to 0, i.e. load always satisfied (see Appendix A for details), (2) a minimum allowed self-sufficiency ratio (SSR) constraint measured as the percentage of demand served by local distributed energy resources over the one-year operation of the system (Eq. (9)) [75], which is set to 80%, (3) a terminal energy in store constraint, which ensures that the state-of-charge (SOC) of the battery storage system at the end of the year-long operating horizon equals or exceeds its initial energy content (Eq. (10)), and (4) specific upper bounds on the decision variables (sizes of the components), in compliance with physical, real-world limitations (Eq. (11)).

$$LPSP \leq LPSP^{max}, \tag{8}$$

$$SSR \geq SSR^{min}, \tag{9}$$

$$E_B(T) \geq E_B(0), \tag{10}$$

$$0 \leq N_c \leq N_c^{max}. \tag{11}$$

2.3. Nested MG scheduling optimisation

In contrast to the rule-based, hourly-basis dispatch strategy commonly employed in the MG design optimisation software packages and most of the existing MG sizing methods in the literature (to charge the storage when excess renewable power is present and to discharge the storage when renewable sources are not satisfying the load demand), the proposed algorithm accommodates an intelligent scheduling optimisation algorithm nested within the optimal sizing problem. The scheduling optimisation is formulated as a LP problem solved using the built-in 'linprog' MATLAB function over a moving 24-hour time horizon. Mathematically, the optimal scheduling problem can be expressed as [76]:

$$\min \boldsymbol{OPEX} = \boldsymbol{P_{im}}\boldsymbol{\pi}^T \Delta t - \boldsymbol{P_{ex}}\boldsymbol{\pi}^T \Delta t + 10^{-6}\|\boldsymbol{u}\|_1, \tag{12}$$

subject to:

$$\boldsymbol{P_{im}} - \boldsymbol{P_{ex}} = \boldsymbol{P_L} - \boldsymbol{P_{PV}} - \boldsymbol{P_{WT}} + \boldsymbol{P_{ch,B}} - \boldsymbol{P_{dch,B}}, \tag{13}$$

$$E_B(t) = E_B(t-1).\left(1 - \sigma_B.\Delta t\right) + \eta_{ch,B}.P_{ch,B}(t).\Delta t - \frac{P_{dch.B}(t).\Delta t}{\eta_{dch,B}} \ \forall t, \tag{14}$$

where $\boldsymbol{OPEX}$, $\boldsymbol{P_{im}}$, $\boldsymbol{P_{ex}}$, $\boldsymbol{\pi}$, $\boldsymbol{P_L}$, $\boldsymbol{P_{PV}}$, $\boldsymbol{P_{WT}}$, $\boldsymbol{P_{ch,B}}$, and $\boldsymbol{P_{dch,B}}$ denote the 24-hour column vectors of the daily operational expenditure, imported power, exported power, wholesale electricity price, load demand, solar PV power output, WT power output, battery charging power, and battery discharging power, respectively; $10^{-6}\|\boldsymbol{u}\|_1$ represents the L1-norm of the battery schedules over the 24-hour operational horizon that is included to penalize any needless battery cycling; E_B is the energy content of the battery bank; $\eta_{ch,B}$ and $\eta_{dch,B}$ respectively denote the battery charging and discharging efficiencies (92%); σ_B is the battery self-discharge rate (0.3%/day); and Δt is the length of each time-step (1 hour).

The objective function is, additionally, subject to a secondary set of operational constraints. Specifically, at the operational level, strictly positive minimum and maximum installed capacity bounds are placed on the operating points of the non-dispatchable renewable energy generation and energy conversion assets Eq. (15)); for the battery bank, this includes lower and upper limits on the energy in store (Eq. (16)), as well as the charge and discharge power capacities (Eqs. (17) and ((18)). The

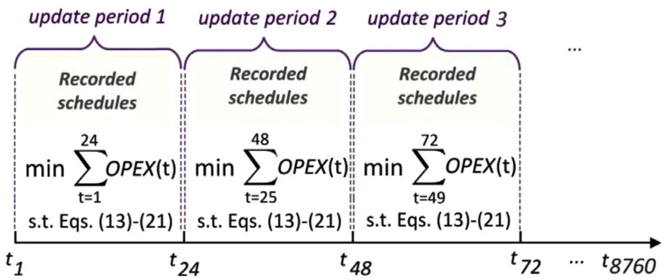

Fig. 2. Structure of solving a sequence of look-ahead optimal scheduling problems over a moving 24-h time window.

upper bounds represent the optimised sizes of the components, whereas the lower bounds are controlled by the corresponding upper bounds. Specifically, the maximum depth of discharge of the battery bank was assumed as 90% [77]. Also, an initial energy in store constraint (Eq. (19)) sets the battery bank to be fully charged at the beginning of the simulations (the first time-step of the MG operation). Moreover, two separate constraints enforce the product of the hourly battery charging and discharging powers, as well as the hourly imported and exported powers to be equal to zero, as behind-the-meter batteries cannot be operated to simultaneously charge and discharge (Eq. (20)), and the transformer at the point of common coupling cannot be operated to concurrently import and export electricity (Eq. (21)).

$$P_c^{min} \leq P_c(t) \leq P_c^{max}, \tag{15}$$

$$E_B^{min} \leq E_B(t) \leq E_B^{max}, \tag{16}$$

$$P_{ch,B}^{min} \leq P_{ch,B}(t) \leq P_{ch,B}^{max}, \tag{17}$$

$$P_{dch,B}^{min} \leq P_{dch,B}(t) \leq P_{dch,B}^{max}, \tag{18}$$

$$E_B(0) = N_B.C_{B,r}, \tag{19}$$

$$P_{ch,B}(t).P_{dch,B}(t) = 0, \tag{20}$$

$$P_{im}(t).P_{ex}(t) = 0. \tag{21}$$

It is worth noting that it is assumed that the MG has a contract with a financially responsible market participant (FRMP), which has financial obligations with respect to their subscribers for energy sold or purchased through the wholesale spot market. This allows the MG to access the wholesale electricity market. Of the various FRMPs working under the existing wholesale market regulatory arrangements, the registered small generator aggregators – which aggregate the outputs of a number of small generating units and dispatch the collective output into the spot market – are particularly well-suited for the purpose of this study.

Fig. 2 illustrates the structure of solving a sequence of day-ahead (24-h) optimal dispatch problems (at an hourly resolution) using the LP-based energy scheduling framework.

2.4. Battery degradation

The battery degradation over its lifetime is modelled using two variables, each of which represents a fractional capacity loss (from 0 when new to 0.2 at the end of its life for a 20% capacity degradation limit), namely: the calendar and cycling degradation. The battery capacity fade is defined as the maximum of the two values. That is, the battery's end of life is determined by the calendar or cycling degradation, whichever is greater.

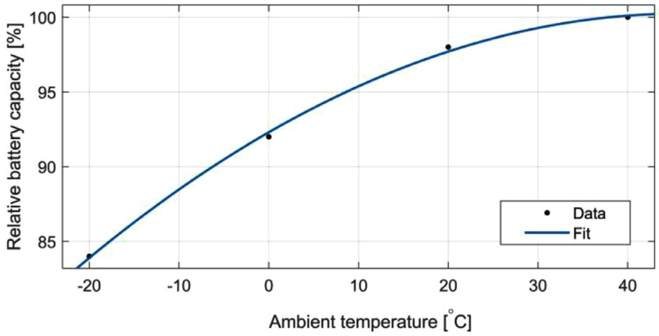

Fig. 3. Fitting a second-degree polynomial curve to the relative battery capacity versus temperature data.

The calendar-induced degradation, the rate of increase of which depends on the operating temperature, is modelled as [78]:

$$kt = B \times e^{-\frac{d}{T_i}}, \tag{22}$$

where kt denotes the rate of increase of the calendar degradation variable, B (2.28×10^{-6}) and d (0) are the manufacturer-provided constants fit to empirical data, and T_i is the battery's internal temperature [K], which can be calculated as [78]:

$$T_i(t+1) = (T_i(t) - T_a(t) - \frac{\dot{Q}}{h})e^{-\frac{h}{mc}\Delta t} + \frac{\dot{Q}}{h} + T_a, \tag{23}$$

where T_a is the ambient temperature [K], m is the mass of the battery (9.08 kg per 1 kWh pack), c is the specific heat capacity (800 J/kg-K), h is the thermal conductance to ambient temperature (10 W/K), and $\dot{Q}$ ($\dot{Q} = \frac{V^2}{R}$) denotes the losses in the series resistance that are converted to heat, with V representing the battery pack's nominal voltage (3.7 V) and R denoting its effective series resistance (3.6×10^{-4} ohms).

The battery is enforced to operate within an allowable internal temperature range, as:

$$T_i^{min} \le T_i \le T_i^{max}, \tag{24}$$

where T_i^{min} and T_i^{max} are the minimum and maximum internal operating temperature limits of the battery, which are fixed at 0 °C and 60 °C, respectively.

Furthermore, the mathematical model of the battery includes variation in capacity with temperature, which can be formulated as follows:

$$C_B(T_a) = C_{B,r} \times \left(d_0 + d_1 \times T_a + d_2 \times {T_a}^2\right), \tag{25}$$

where T_a is the ambient temperature-dependent relative capacity of the battery, $C_{B,r}$ is the rated capacity of the battery, while d_0, d_1, and d_2 are the coefficients obtained from fitting a second-degree polynomial curve to the manufacturer-provided relative capacity versus ambient temperature data (Fig. 3), which are respectively fixed at 9.23×10^{-1}, 3.45×10^{-3}, and -3.75×10^{-5}.[4]

Moreover, the cycle fatigue on the battery is modelled by the following equation [78]:

$$1/N = A \times DOD^{\beta}, \tag{26}$$

where N is the number of cycles to failure, DOD is the depth of discharge, while A (1.44×10^{-4}) and β (1.79) are fitted constants.

The rainflow cycle counting algorithm [79] is utilised to convert the battery's one-year SOC profile into a set of discrete cycles with the corresponding depth of discharge values. To this end, the built-in 'rainflow' MATLAB function is used. Then, the total (cumulative) cycle-life degradation is determined as:

$$D = \sum_{i=0}^{N} A \times D_i^{\beta}. \tag{27}$$

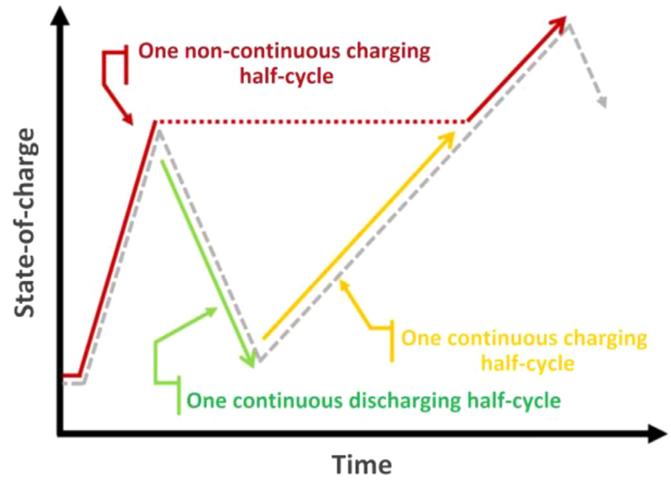

Fig. 4. Illustrative example of the rainflow cycle counting algorithm (adapted from [80]).

Fig. 4 shows an illustrative example of the rainflow algorithm applied to a representative battery SOC profile [80]. The figure demonstrates three half-cycles; the red arrow represents a non-continuous charging half-cycle, while the green and yellow arrows respectively represent continuous discharging and charging half-cycles that are of the same cycle depth.

It should also be noted that the battery bank is limited by the charging and discharging power capacities, which are both fixed at C/2, meaning that the battery bank can be fully charged or discharged in two hours.

2.5. Moth-flame optimisation algorithm

The search and selection of the cost-minimal MG configuration consist of an application of a modified version of the MFOA to the objective function derived in Eq. (1). The MFOA is a state-of-the-art, nature-inspired, population-based metaheuristic that systemically rebalances exploration (i.e., the early stages of the optimisation process that mimics the long-range movement of individuals) for improved exploitation (i.e., the local search around promising regions) of the search space for potential solutions. The MFOA simulates the navigation system of moths at night – referred to as 'transverse orientation'. It considers both the moths and flames as search agents and is one of a few meta-heuristics that makes use of two types of search agents, whereby the exploration and exploitation are traded off as the search progresses. More specifically, the moths represent the individuals that search the design space, whereas the flames are the pins dropped by the moths to keep a track of the best solution obtained over the course of iterations.

In this algorithm, the relationship between the moths and flames is modelled using the following equation [56]:

$$M_i = S\left(M_i,\ F_j\right), \tag{28}$$

where M_i and F_j respectively represent the position of the i-th moth and j-th flame, while S is a logarithmic spiral function that directs the search, which can be defined as follows:

$$S\left(M_i,\ F_j\right) = D_{ij} e^{bt} \cos(2\pi t) + F_j, \tag{29}$$

where D_{ij} indicates the distance between the i-th moth and the j-th flame that can be calculated by Eq. (30), b is a constant that defines the

[4] Although increasing the number of observed data points results in narrowing the gap between the confidence band and the best-fit curve, improving the accuracy of input data has been deemed secondary for the goal of demonstrating the utility and effectiveness of the proposed MG equipment capacity-planning method.

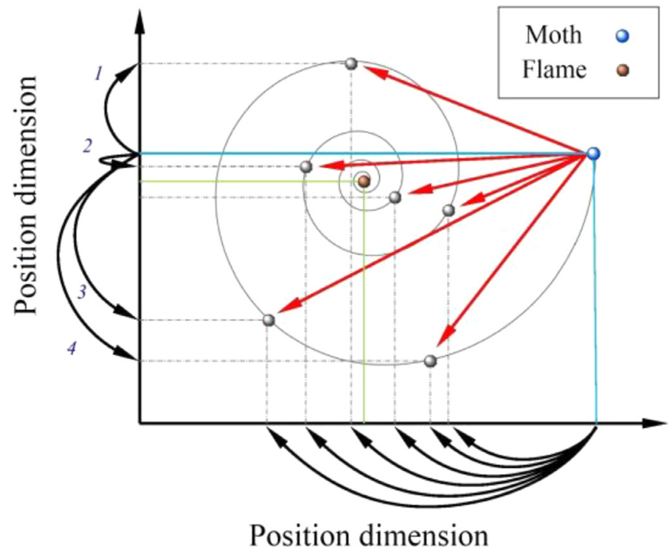

Fig. 5. Conceptual illustration of the exploration-exploitation trade-off ability of the MFOA (adapted from [56]).

shape of the logarithmic spiral, and t is a random number in the range $[-1, 1]$ that controls the degree of closeness of the moths with respect to flames in the next iteration.

$$D_{ij} = \left|F_j - M_i\right|. \tag{30}$$

Furthermore, to reduce the probability of local optima stagnation, each moth is constrained to update its position with respect to only one flame.

This procedure continues iteratively until the maximum number of iterations, as the stopping criterion, is reached. Finally, the best individual's fitness value (return value of the objective function) in the last iteration of the algorithm is reported as the optimal value of the objective function over the feasible region of the optimisation problem.

Fig. 5 provides a conceptual illustration of the update process of the MFOA, where the grey dots represent the next possible solutions of a hypothetical problem (i.e., a representative moth's possible positions in the next iteration). As the figure shows, the MFOA is able to adaptively trade-off the exploration and exploitation. Specifically, the algorithm exploits the search space if the corresponding flame is in the vicinity of the moth (as labelled by arrow 2 in the figure), otherwise, it explores the design space (as indicated by arrows 1, 3, and 4).

2.5.1. Lévy-flight MFOA

The Lévy-flight MFOA was initially introduced by Li et al. [70]. In mathematics, the Lévy-flight is a random walk in that the step-lengths are Lévy-distributed – a heavy-tailed probability distribution. Equipping the original MFOA with the Lévy-flight mechanism has been found to improve the diversity of the population of individuals necessary to avoid premature convergence. Specifically, Lévy flights are composed of clusters of multiple short steps connected by longer relocations (see Fig. 6) [81].

The main principle of the Lévy-flight MFOA is to let each moth perform one Lévy-flight after updating its position, which can be formulated as [70]:

$$X_i^{t+1} = X_i^t + u\ \mathrm{sign}[\mathrm{rand} - 0.5] \oplus \mathrm{Levy}(\beta), \tag{31}$$

where X_i^t is the position of the i-th moth at the t-th iteration, u is a random number drawn from a uniform (0,1) distribution, the term $\mathrm{sign}[\mathrm{rand} - 0.5]$ takes on one of the three values of −1, 0, and 1, ⊕ denotes the element-wise product, while $\mathrm{Levy}(\beta)$ is defined as follows [70]:

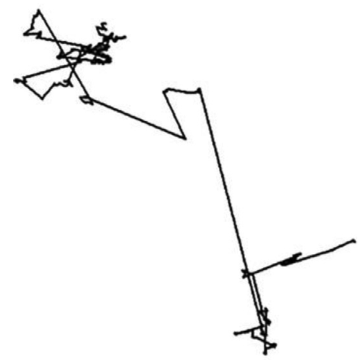

Fig. 6. Illustrative example of Lévy flights [81].

$$\mathrm{Levy}(\beta) \sim \frac{\emptyset \times \mu}{|v|^{\frac{1}{\beta}}}, \tag{32}$$

where μ and v are random numbers drawn from a standard normal distribution, β is a parameter that is fixed at 1.5, while ∅ is defined as follows [70]:

$$\emptyset = \left[\frac{\Gamma(1+\beta) \times \sin\left(\frac{\pi\times\beta}{2}\right)}{\Gamma\left(\left(\frac{1+\beta}{2}\right) \times \beta \times 2^{\frac{\beta-1}{2}}\right)}\right]^{1/\beta}, \tag{33}$$

where Γ is the standard gamma function, computed using the built-in 'gamma(X)' MATLAB function.

2.6. Overview of the proposed model

Fig. 7 illustrates the general meta-heuristic-based MG capacity planning solution algorithm with nested optimal energy dispatch strategy. As the figure shows, the overall problem is formulated as an outer loop capacity planning optimisation problem, within which daily optimal energy management problems are nested. The simulation process, in which component sizes are treated as 'here-and-now' variables and the operating schedules serve as 'wait-and-see' variables, is described in more detail along the following steps:

1 The Lévy-flight MFOA's population of candidate solutions (to the optimal sizing problem with the objective function defined in Eq. (1)) is randomly initialised subject to the imposed component-specific maximum allowable capacity constraint (Eq. (11)) at the capacity planning level, and then passed to the inner operational planning loop.
2 For each search agent in the inner loop, the optimal daily operating strategy is determined until the operating schedules have been developed for the whole representative operation period (one year) and the obtained results are returned to the outer loop. To this end, the optimal dispatch problem with the objective function defined in Eq. (12) is solved subject to the operational-level constrains in Eqs. (13)–(21), whilst additionally accounting for the calendar and cycling-driven battery degradation components using Eqs. (22)–(27). This provides a platform to check whether the non-maximum-capacity-related constraints at the planning level Eqs. (8)–((10)) are relaxed.
3 The return values of the investment planning objective function (Eq. (1)) are calculated to evaluate the fitness of each candidate solution.
4 The outer design process will loop with the updated positions of the dedicated search agents until any of the termination conditions are met. Specifically, additionally to the main iteration counter, $Iter$, an auxiliary iteration counter, Num, is defined, which serves as an

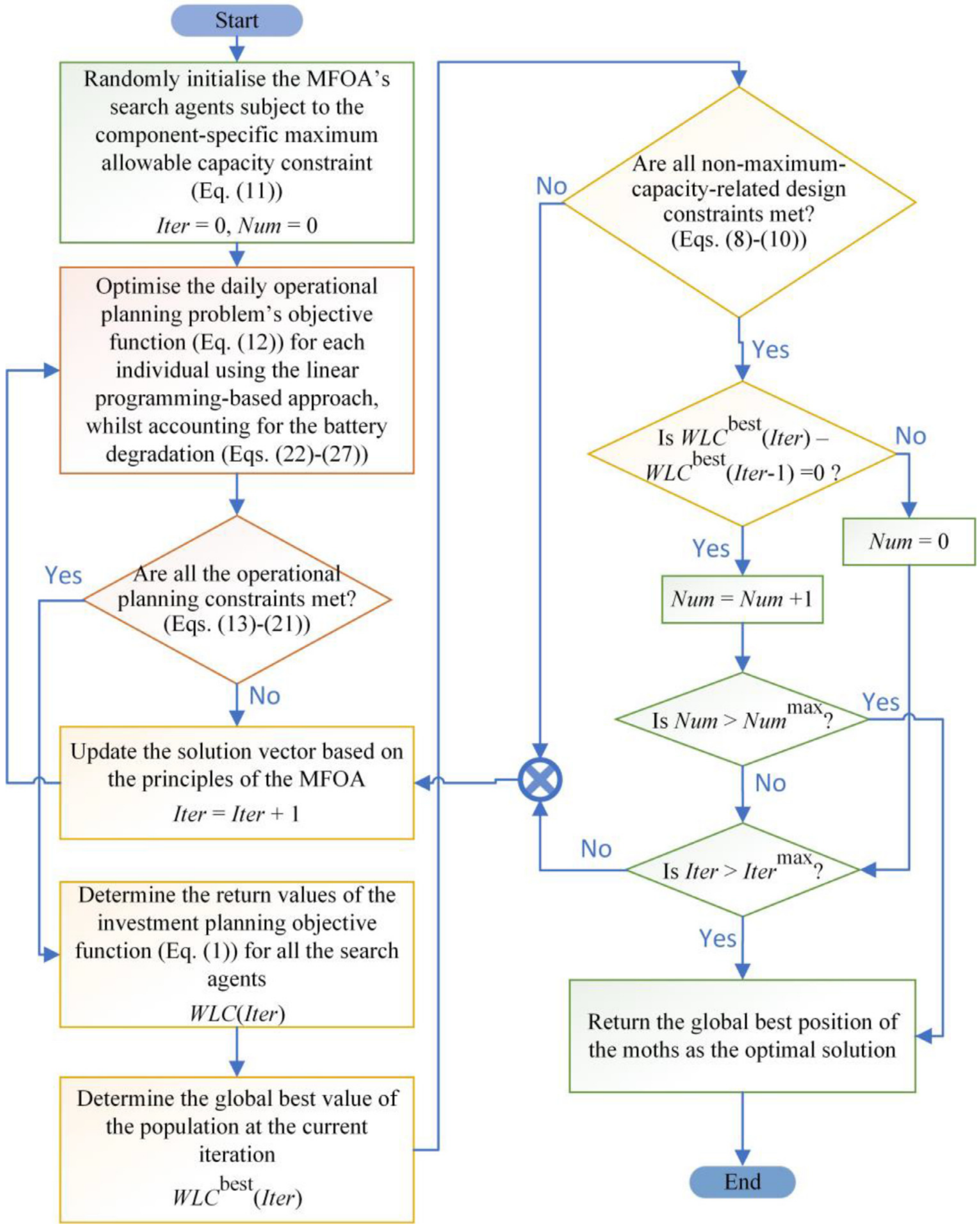

Fig. 7. Meta-heuristic-based solution approach for MG capacity planning problem with nested optimal operational scheduling.

adaptive stopping criterion. The auxiliary counter helps speed up the simulation process by terminating the equipment size selection loop if the fitness of the outer loop capacity planning objective function has not improved over a pre-defined number of iterations, denoted by Num^{max} (in this paper, $Num^{max} = 50$). If the auxiliary counter has not reached the maximum value, the iteration limit set for the main counter, denoted by $Iter^{max}$ (in this paper, $Iter^{max} = 200$) controls the termination of the programme.

3. Test-case system model

The grid-connected, DC-coupled community MG, shown in Fig. 8, is modelled for an eight-lot residential subdivision, namely Totarabank, which is located in the Wairarapa District of the North Island of New Zealand (see Fig. 9). Designed based on permaculture principles, Totarabank is a small resilient eco-community committed to sustainable rural living, with 14 inhabitants [82,83]. The energy flow through the MG components was modelled without losses. However, conversions from AC to DC, from DC to AC, and from DC to DC, were assumed to have efficiencies of 96% for each direction [84]. Also, the transformer's round-trip efficiency for exchanges with the AC grid was assumed to be 94% [85]. The optimal sizes of the power conversion devices serving as interfaces between the MG components and the common DC bus are dependent on the optimal sizes of the corresponding energy generation/storage components. That is, out of the power electronics devices, only the size of the multi-mode (hybrid) system inverter is determined independently. Additionally, the real interest rate is assumed to be 2.45% [86] and the system is expected to last 20 years.

The following section mathematically models the distributed energy generation and storage technologies of the MG system.

3.1. PV panels

The power output from each PV panel in time t is [87]:

$$P_{PV}(t) = \eta_{PV}(t).a_{PV}.I_G(t), \quad (34)$$

$$\eta_{PV}(t) = \eta_r + (1 - \beta\left(T_c(t) - T_{c,ref}\right), \quad (35)$$

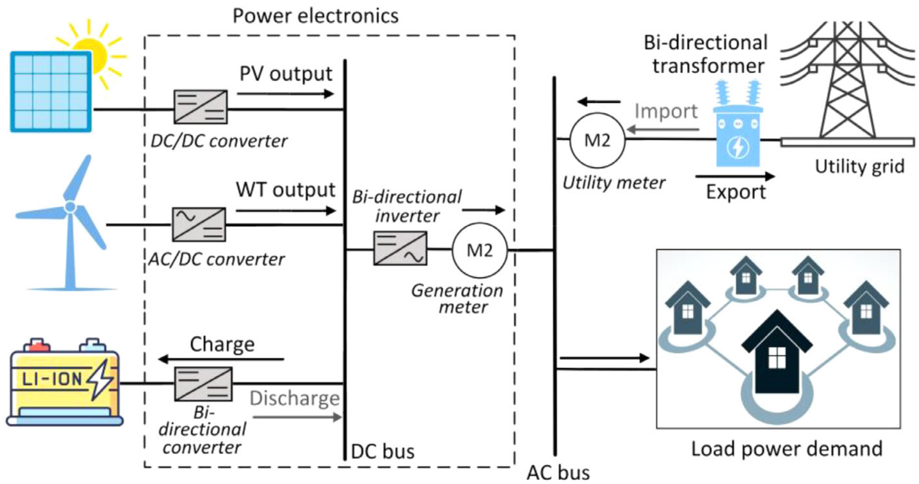

Fig. 8. Schematic of the conceptual grid-tied, DC-coupled solar PV/WT/battery community MG system.

Fig. 9. Case study site: (a) location on a New Zealand satellite map (GPS coordinates: 41°1′4” S 175°40′0” E); (b) satellite photograph with subdivision lots overlaid (image courtesy of Google Earth).

$$T_c(t) = T_a(t) + \left(\frac{NOCT - 20}{0.8}\right) I_G(t), \tag{36}$$

where $\eta_{PV}(t)$ is the time-variant efficiency of the panel, a_{PV} is the panel's area (1.64 m^2), $I_G(t)$ is the global horizontal solar irradiance in time t [kW/m^2], η_r is the panel's rated efficiency (17.4%), β is the PV temperature coefficient of power (−0.48%/°C), T_c is the cell temperature, $T_{c,ref}$ is the reference cell temperature (25 °C), T_a is the ambient temperature [°C], and $NOCT$ denotes the nominal operating cell temperature (43 °C).

3.2. Wind turbines

The power output from each WT is given by [16]:

$$P_{WT}(t) = \begin{cases} 0 \text{ if } v(t) \le v_{ci} \text{ or } v(t) \ge v_{co}, \\ A \text{ if } v_{ci} < v(t) \le v_r, \\ P_{WT,r} \text{if } v_r < v(t) < v_{co}, \end{cases} \tag{37}$$

$$A = \frac{P_{WT,r}}{v_r^3 - v_{ci}^3} v^3(t) - \frac{v_{ci}^3}{v_r^3 - v_{ci}^3} P_{WT,r}, \tag{38}$$

where $v(t)$ denotes the wind speed in time t, v_{ci} is the WT's cut-in wind speed (2.7 m/s), v_r is the WT's rated wind speed (11 m/s), v_{co} is the WT's cut-out wind speed (25 m/s), and $P_{WT,r}$ is the selected turbine's rated power (5 kW).

Fig. 10 displays the monthly mean 24-h profiles for the forecasted power load, solar irradiance, ambient temperature, wind speed, and wholesale electricity price. The forecasted meteorological and wholesale electricity market price profiles were derived by taking an average over the years of 2010 to 2019 from data provided by the New Zealand's National Institute of Water and Atmospheric Research [88] and the New Zealand Electricity Authority [89], respectively. Also, the power load profile was synthesised based on the New Zealand GREEN grid project's estimates of the future household demand profiles in accordance with the site's population and household size [90]. Note that figures depict New Zealand time for the relevant month. As the associated profiles in Fig. 10 suggest, (1) low-grade heat uses are electricity dominated, implying that load peaks on long dark cold winter nights, (2) the case study site is well-endowed with solar PV and wind resources, which have complementary diurnal and seasonal production profiles – wind higher at night and in winter, solar PV higher in the daytime in summer, and (3) in the context of New Zealand's hydro-dominated system, spot electricity prices are typically higher during the drier summer months when hydro lakes (storage) and inflows are below average and the back-up role is primarily filled by more expensive natural gas-fired and coal power plants.

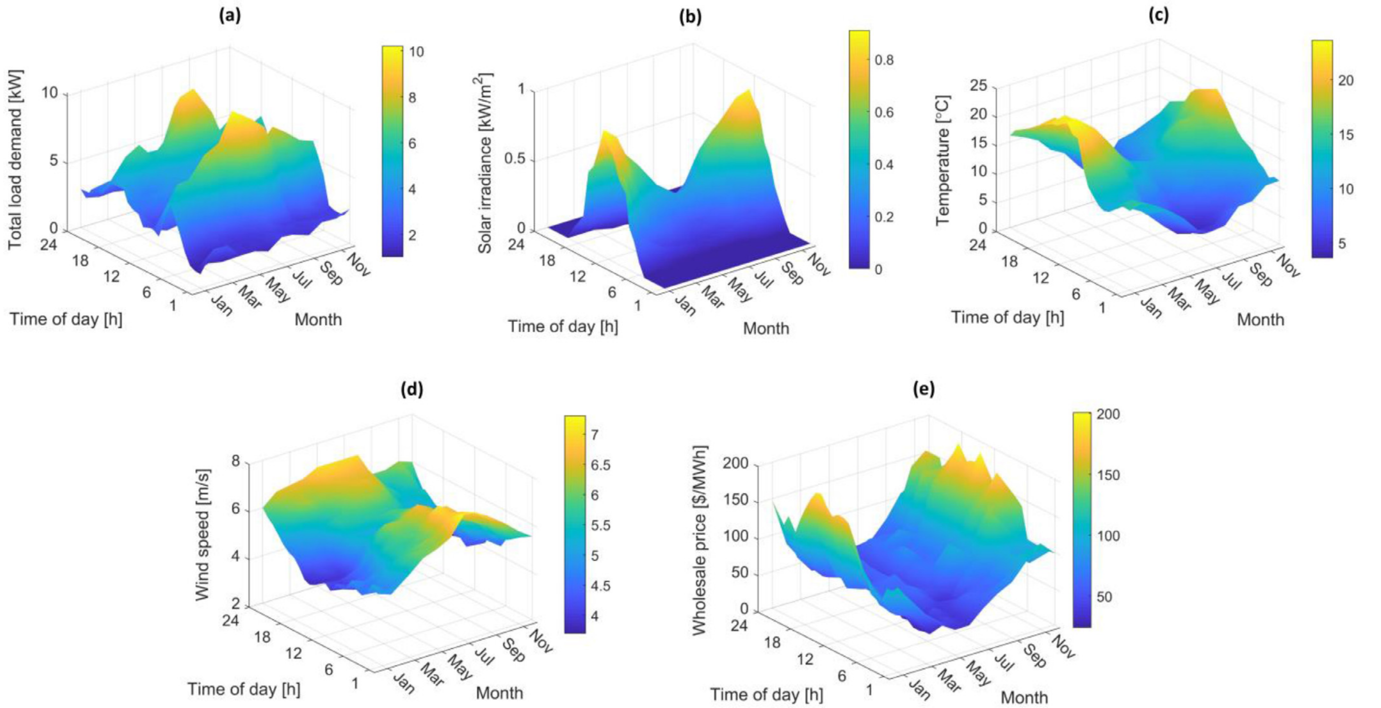

Fig. 10. Monthly mean daily profile for: (a) load demand; (b) solar irradiance; (c) ambient temperature; (d) wind speed; (e) wholesale electricity price.

Table 3
Data values and sources for the techno-economic specifications of the MG system.

Component	Nameplate rating	Capital cost	Replacement cost	O&M cost[a]	Lifetime	Efficiency	Source
PV panel	375 W (Canadian Solar KuMax)	$437/unit	N/A[b]	$1.9/unit/yr	20 years	18.9%	[91]
Wind turbine	5 kW (AWS HCM)	$6,450/unit	N/A[b]	$28/unit/yr	20 years	N/A[c]	[92]
Battery pack	1 kWh (Generic)	$885/kWh	$417/kWh[d]	$2.1/kWh/yr	15 years or 12,000 cycles[e]	92%[f]	[84]
Hybrid inverter	3 kW (Selectronic SPMC240)	$4,600/unit	$4,600/unit[g]	$3.9/unit/yr	15 years	96%	[93]

[a] Estimated based on the capital-to-O&M cost ratios presented in [94,95] for the relevant technologies.
[b] Not applicable, as no replacement is needed over the analysis period.
[c] Not applicable, as the power output from the wind plant is adaptively estimated based on wind speed (see Eq. (37)).
[d] Estimated based on cost projections from the Australia's National Science Agency for behind-the-meter Li-ion batteries [96].
[e] Estimated considering a depth of discharge of 100%.
[f] Charge and discharge efficiencies.
[g] No significant change is projected for the costs of power electronics devices [84].

It is assumed that low-temperature heat is the main source of household electrical energy use. Specifically, it collectively amounts to 46% of the total electricity use, of which 27% is used for space heating and 19% is used for water heating. Also, residential appliances account for 54% of the total household electricity use, with the breakdown as follows: plug-load appliances (19%); refrigeration (15%); lighting (12%); and range (8%). Note that the above percentage points represent the associated total annual electricity uses, which are to a great degree subject to seasonality.

Also, Table 3 lists the data values and sources for the MG equipment techno-economic parameters. Note that, in this paper, all monetary values are expressed in 2019 NZ$; where required, foreign currencies were converted into NZ$ at the yearly average currency exchange rates in 2019.

4. Simulation results and discussion

The results associated with the application of the developed model to the test-case are presented in this section. The section begins by providing a comparative evaluation of the performance of the proposed model with that of the leading pre-feasibility design software for modelling MGs, HOMER Pro, for initial validation (Section 4.1). It then demonstrates the superiority of the Lévy-flight MFOA to the basic MFOA, as well as eight well-established and state-of-the-art meta-heuristics in the literature, when embedded in the proposed meta-heuristic-based MG capacity planning solution approach (Section 4.2). The section then proceeds to focus explicitly on the system optimised by the Lévy-flight MFOA with representative energy balance analyses (Section 4.3), cash flow analyses (Section 4.4), capital budgeting analyses (Section 4.5), and a specific sensitivity analysis (Section 4.6).

4.1. Model validation

To validate the effectiveness of the model in estimating the globally optimum MG sizing solutions, the results are benchmarked against the design of a similar system using HOMER Pro. In order to precisely match the proposed model to a model in HOMER Pro, the power output from solar PV and WT calculations used in HOMER Pro [97,98] were adopted in the proposed model. Fig. 11 shows the layout of the HOMER Pro model.

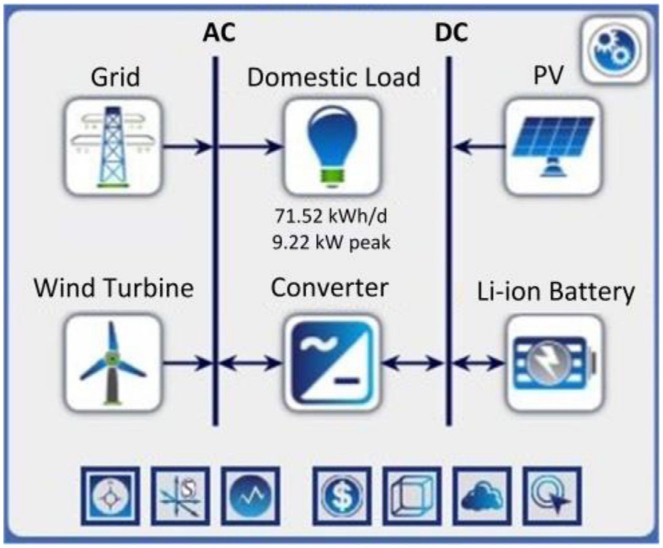

Fig. 11. HOMER Pro model of the MG used for benchmarking.

Table 4 presents a direct comparison of the proposed modelling and HOMER Pro results.

Fig. 12 provides a statistical representation of the hourly change in the SOC of the Li-ion battery bank over a one-year operation of the optimally sized system. The boxplots show the interquartile range of the battery SOC with the lines that divide the boxplots into two parts representing the median of the relevant data. The whiskers represent the most extreme data points (minimum and maximum values) obtained from the simulations. A smaller distribution of the battery SOC, as described by the boxplots, indicates that the hourly data are more condensed. Note that a positive value represents an increase (charging mode) in the battery SOC, negative a reduction (discharging mode).

Figs. 13 and 14 respectively show the monthly mean profiles for the energy purchased from the grid and energy sold back to the grid in the optimal solution sets determined by the proposed Lévy-flight MFOA-based model and HOMER Pro.

The comparative results presented in Table 4, as well as Figs. 12–14 are collectively revealing in several ways. First, while HOMER Pro selected a battery-less MG configuration as the optimum solution, the proposed meta-heuristic model determined the optimal size of the Li-ion battery bank to be 41 kWh. However, the sum of the sizes of the local renewable energy generation technologies in the cost-optimal equipment capacity combination has remained unchanged. The reason for this is that the sum of the optimal sizes of the solar PV panels and WTs is found to be the maximum permissible amount that meets the existing installed transformer's capacity constraint in both cases. That is, given the intra-day volatility in the New Zealand Wholesale Electricity Market that ranges from 6% to 28%, both the solution algorithms agree that it is cost-optimal to build the largest possible renewable energy generation capacity, provided that the upstream grid acts as an infinite bus absorbing any injected power subject to the transformer capacity. Collectively, the optimally selected and sized renewable energy assets (for minimum life-cycle cost) by the meta-heuristic-based model indicated an increase of approximately 18% in the total net present value of the project. The key insight arising from this observation is that the meta-heuristic-based solution algorithm explores the solution space more effectively than the seemingly exact mathematical solution algorithms – which require high-order linear approximations of the objective function in MG planning applications.

Second, while the solution optimised by the meta-heuristic-based algorithm did not choose to use the energy arbitrage strategy in its classic definition of 'charge cheaply, discharge discreetly', the comparative year-round profiles for the energy exchanged with the grid (see Figs. 13 and 14), as well as the summary statistics of the optimal battery charging/discharging strategies adopted at the corresponding time-steps in the Lévy-flight MFOA-optimised solution (see Fig. 12), indicate that the solution algorithm has implemented an intelligent energy trading scheme – as part of the optimum solution. Specifically, the LP optimisation-based day-ahead energy dispatch strategy integrated into the proposed model decided to supply part of the demand by importing from the utility grid during off-peak periods when wholesale prices are lower; the excess on-site renewable energy generation is stored to be discharged later for on-site use when wholesale prices are higher. In this way, the arbitrage economics of energy storage are valued in-

Table 4
Comparative Lévy-flight MFOA-based model and homer pro results.

Output	Optimisation method Proposed model	HOMER Pro
Total net present cost of the MG[a] [$]	−50,332	−42,646
Total discounted renewable energy generated [kWh]	2,458,206	2,407,175
LCOE[b] [$/kWh]	−0.020	−0.018
PV size [kW]	17.5	7.5
WT size [kW]	30	40
Battery size [kWh]	41	0
System inverter size [kW]	9	15
Total equipment-related costs [$]	123,012	95,763
Total net energy purchased [kWh]	−1,404,360	−1,120,469
Total net electricity exchange costs [$]	−173,344	−138,409
Total renewable energy curtailed [kWh]	0	19,620
Grid outage survivability [%]	100%	100%
Battery bank autonomy [h]	14	0
CPU usage time [s]	122,517	2,409

[a] The net present cost is the negative of the net present value; that is, a negative total net present cost indicates that the projected revenues generated by the project exceed the total expected costs. Refer to Section 4.5.4 for a more detailed discussion on this outcome.

[b] The levelised cost of energy (LCOE) is defined as the total net present cost of the MG divided by the total discounted electrical power load served including exports, which equals the total renewable energy generated under the assumptions made in this paper. Refer to Section 4.5.4 for a more detailed discussion on this outcome.

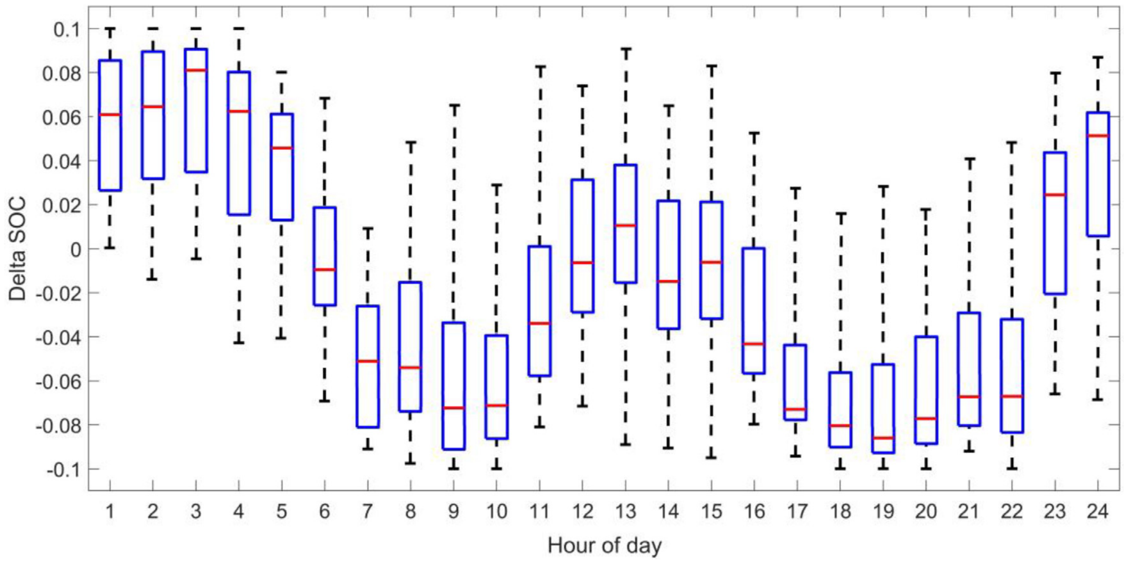

Fig. 12. Summary statistics for the energy content of the battery bank over the year [kWh].

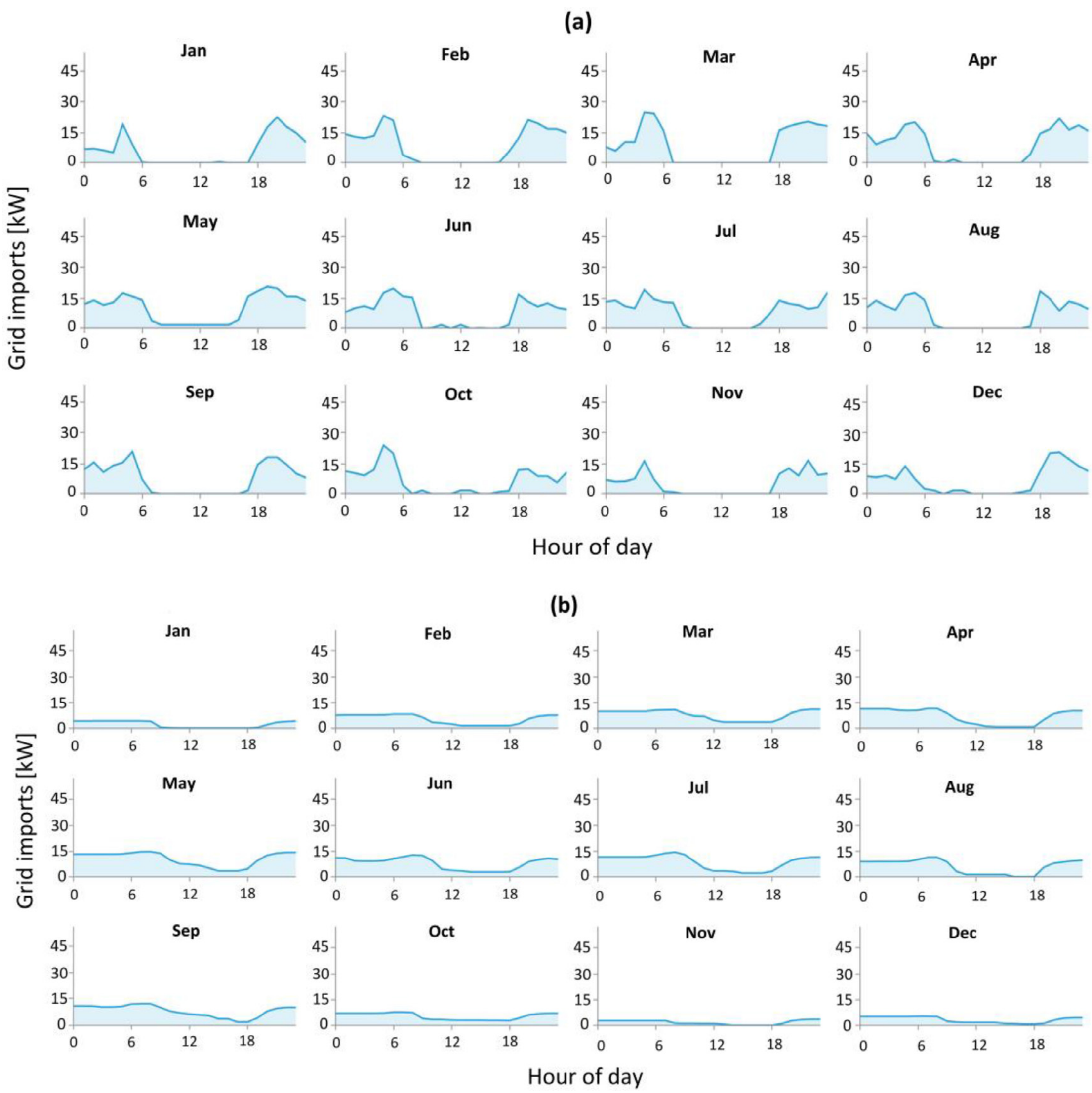

Fig. 13. Monthly mean profile for the energy imported from the grid: (a) proposed model; (b) HOMER Pro.

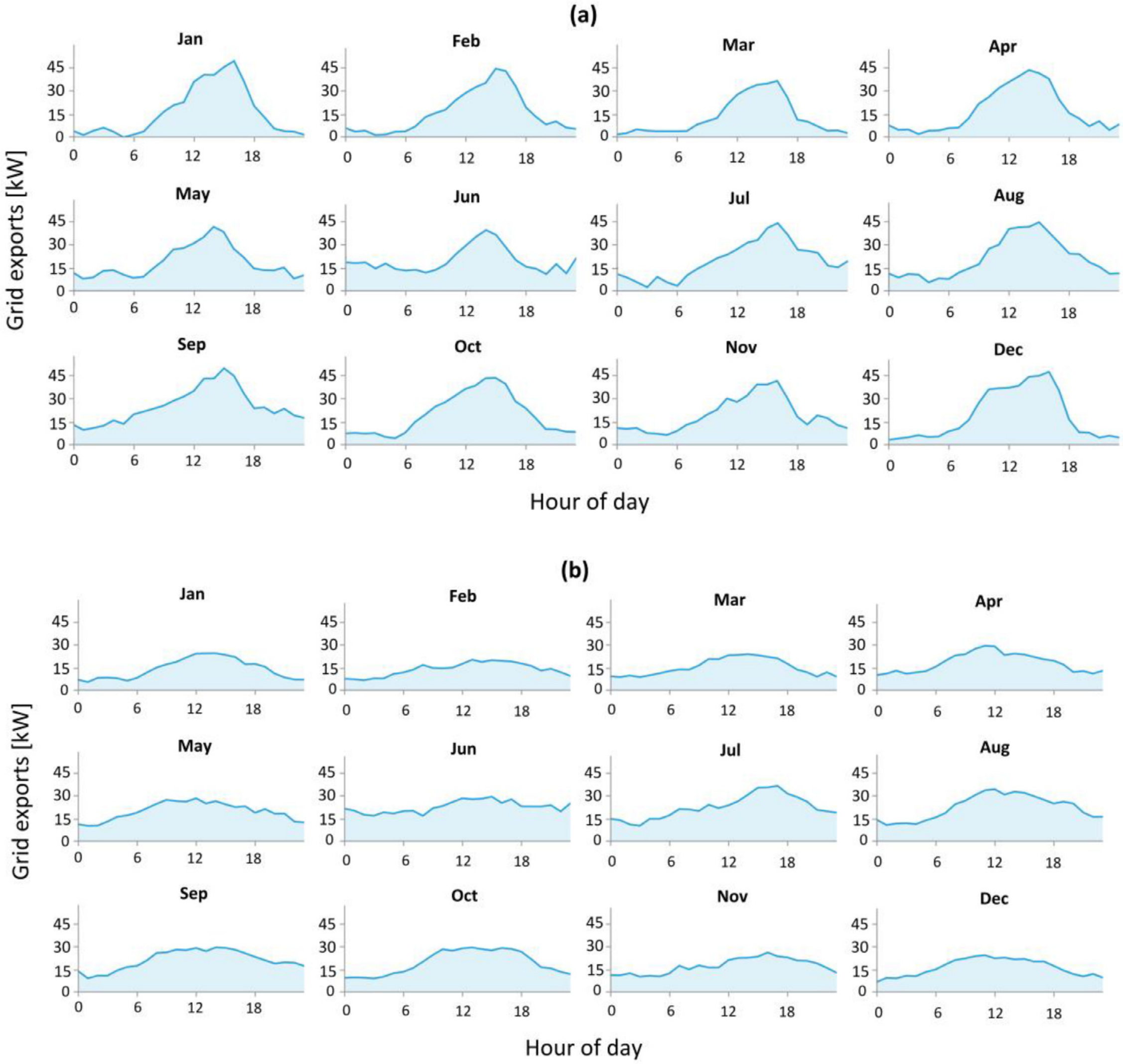

Fig. 14. Monthly mean profile for the energy exported to the grid: (a) proposed model; (b) HOMER Pro.

directly. In contrast, the rule-based Greedy energy dispatch algorithm[5] [84] has failed to make effective use of the storage capacity as a hedge against the daily volatility in wholesale electricity market prices; this is the main underlying reason for the selected battery-less MG configuration by HOMER Pro.

Third, the presence of the battery bank in the optimal solution set yielded by the Lévy-flight MFOA-based solution algorithm provides direct benefits in terms of energy resilience. Specifically, the MG resilience to grid outages and on-site renewable power disruption was quantified using two indices, namely: the grid outage survivability (the ratio of the battery bank capacity to the annual mean 'net' power load) [100], and the battery bank autonomy hour (i.e., the ratio of the battery bank capacity to the annual mean power load) [101]. Both the methods yielded a grid outage survivability of 100%, meaning that both the battery-less and battery-integrated optimised systems are able to sustain electrical loads for the site during indefinite grid outages. While the two systems have the same resilience benefit in terms of an outage on the grid, the cost-minimal system determined by the Lévy-flight MFOA-based solution algorithm is, additionally, able to sustain electrical loads for 14 hours of a more severe outage that disrupts access to the electricity generated from the on-site renewable resources and the grid (using solely the battery backup power) – with a higher total net present worth. Moreover, the inclusion of the battery bank has led to a significant reduction in the curtailment of non-dispatchable power (solar PV and wind). Specifically, while the total excess renewable energy curtailed in the HOMER Pro-optimised system is found to be 19,620 kWh (over the project life-cycle), no curtailment occurs in the system optimised by the proposed model. The curtailment reduction is explained by the ability of the battery-backed system to store the excess renewable power beyond the capacity of the existing installed transformer.

Fourth, the model has yielded a more well-balanced mix of the candidate renewable energy generation technologies. Specifically, while the optimal generation capacity mix is found to be 84% wind and 16% solar PV by HOMER Pro, the optimum capacity mix determined by the proposed model is 63% wind and 37% solar PV. In large part, this is achieved by the forward-looking characteristic of the intelligent day-ahead scheduling design, which leverages battery storage to cost-optimally address the future non-dispatchable renewable energy shortfalls. In contrast, the rule-based energy dispatch strategy used in HOMER Pro is to sequentially determine the energy schedules at each time step that is linked to other time steps merely through the energy content of the battery bank. Crucially, the look-ahead energy scheduling provisions nested within the proposed capacity planning framework have enabled

[5] Under the Greedy energy scheduling approach, any excess local renewable power generation is used to charge the dedicated battery bank before being exported, whereas any on-site resource deficiency is met by releasing the energy in store before purchasing from the wholesale market.

Table 5
Parameter settings for the meta-heuristics under evaluation.

Algorithm	Parameter settings	Reference
GA	Mutation rate = 0.05, crossover probability = 0.1, mutation probability = 0.9	[28]
PSO	Acceleration coefficients = 2, inertia weight = 0.7	[27]
Hybrid GA-PSO	Mutation rate = 0.05, crossover probability = 0.1, mutation probability = 0.9, Acceleration coefficients = 2, inertia weight = 0.7	[29]
MFOA	$b = 1$	[56]
Lévy-flight MFOA	$b = 1$, $\beta = 1.5$	[70]
HS	Harmony memory accepting rate = 0.85	[30]
SA	Initial acceptance probability = 0.4, cooling ratio = 0.95, size factor = 16, imbalance factor = 0.05	[31]
ABC	Number of onlooker beers = 25, number of employed bees = 25	[32]
ACO	Archive size = 50, locality of search = 0.1, convergence speed = 0.85	[33]
ALO	Self-adaptive adjustment of a single control parameter	[34]

Table 6
Summary statistics for the efficiency comparison of the selected meta-heuristics in terms of the MG whole-life cost.

Algorithm	Best WLC_{MG}	Score	Worst WLC_{MG}	Score	Mean WLC_{MG}	Score	Median WLC_{MG}	Score	SD of WLC_{MG}	Score	Mean score	Rank
Lévy-flight MFOA	**−50,332**	1	−49,716	1	−50,040	1	−49,999	1	175.52	1	1	1
MFOA	−47,244	2	−46,014	2	−46,652	2	−46,718	2	337.76	6	2.8	2
GA	−46,715	4	−45,388	3	−45,741	4	−45,648	4	339.24	7	4.4	3
Hybrid GA-PSO	−46,413	5	−45,219	4	−45,894	3	−45,944	3	355.38	8	4.6	4
PSO	−46,907	3	−45,118	5	−45,684	5	−45,585	5	459.74	9	5.4	5
ALO	−46,114	6	−44,011	7	−44,316	7	−44,273	8	244.01	3	6.2	6
HS	−44,710	9	−44,019	6	−44,297	8	−44,276	7	188.50	2	6.4	7
SA	−44,917	8	−43,880	9	−44,419	6	−44,426	6	295.00	4	6.6	8
ABC	−45,009	7	−43,918	8	−44,253	9	−44,195	9	305.98	5	7.6	9
ACO	−44,588	10	−42,870	10	−43,977	10	−44,076	10	485.57	10	10	10

*Bold indicates the least-cost MG whole-life cost solution obtained across the examined meta-heuristics over 30 independent simulation runs.

the MG to effectively harness the wind-solar complementary seasonal and diurnal cycles with an attendant reduction in excess renewable energy curtailment of 100%, although minimising the renewable energy curtailment was not an optimisation criterion.

Fifth, the ability of the model to search for better results comes at the cost of higher computational requirements. Specifically, a standard desktop computer was able to solve the problem at hand using the HOMER Pro software and the proposed model coded in MATLAB respectively in 2,409 and 122,517 seconds of computational time. Most of the CPU usage time when simulating the proposed modelling framework was in calculating the year-long energy schedules (solving the day-ahead energy dispatch problem) for each of the meta-heuristic individuals at each iteration, taking a total of 98,550 seconds of computational time. The remainder of the CPU usage time (23,967 s) was in updating the positions of moths with respect to flames over the course of iterations. Due to the linearity of the day-ahead energy scheduling problem, a standard desktop computer – with an Intel Core i7 3.20 GHz processor and 16 GB RAM – was able to solve the day-ahead dispatch problem in around 5.4 seconds of computational time (on average), yielding a year-long, daily-basis scheduling optimisation running time of 1,971 s for each moth (search agent).

To further validate the robustness and technical feasibility of the cost-optimal system determined by the proposed Lévy-flight MFOA-based integrated investment and operational planning optimisation approach, a further HOMER model instance was solved using the software's conventional 'grid search' optimisation tool [99].[6] To this end, the set of the decision variable values used by the grid search algorithm to locate the optimal system was defined with reference to the optimal point yielded by the proposed model. More specifically, the list of system component sizes that HOMER considered for the model validation was populated with sizes ranging from 5 units smaller to 5 units greater than the corresponding equipment capacity values returned by the proposed model, with one-unit increments in variables. The HOMER model was then solved for the minimum total discounted system cost. The optimal system design calculated by the grid search algorithm – which is a full-factorial design approach – was found to be exactly the same as that returned by the proposed model, which corroborated the validity of the model. Nevertheless, the resulting total net present value of the MG was found to be ~4% lower than the value generated by the proposed model due to higher net electricity imports. This indicates the efficacy of the operational planning optimisation framework nested within the proposed model, which produces optimal power trading strategies given the forecasts of load, renewable generation, and wholesale prices.

4.2. Benchmarking the Lévy-flight MFOA

In order to verify the superiority of the Lévy-flight MFOA to the basic MFOA, as well as a set of well-established and state-of-the-art meta-heuristics in the MG design optimisation literature – the GA, the PSO, the hybrid GA-PSO, the HS, the SA, the ABC, the ACO, and the ALO – a comprehensive statistical analysis is conducted on their comparative efficiencies when applied to the test-case MG investment planning and capacity optimisation problem at hand.

Table 5 lists the developer-suggested values for the specific control parameters of the meta-heuristics under analysis. For the sake of a fair comparison, the number of dedicated search agents (population size) and the maximum number of iterations were respectively assumed to be 50 and 200 for all the selected algorithms.

Table 6 summarises the descriptive statistics for the performance of the meta-heuristics under analysis and ranks their efficiencies based on the test-case MG whole-life cost results obtained over 30 independent simulation runs – necessary to reach the statistical precision required for the efficiency comparison of meta-heuristics given their approximate nature.[7] Note that computational complexity was not factored into the

[6] The HOMER Pro software has two optimisation algorithms: (1) a conventional 'grid search' algorithm, which simulates all the feasible combinations of the component sizes defined by the 'search space', and (2) a trademarked proprietary derivative-free optimisation algorithm, the 'HOMER Optimizer', which does not require the user to specify all possible options for searching. Unless otherwise noted, the HOMER Pro modelling results presented in this paper represent the results generated by the HOMER Optimizer.

[7] Given the statistical insignificance of the equipment sizing results optimised by the studied meta-heuristics in that no salient differences in terms of MG con-

Table 7
Optimal combination of the MG investment planning decision variables obtained using various meta-heuristics.

Algorithm	PV size [kW]	WT size [kW]	Battery size [kWh]	Inverter size [kW]	Total net electricity exchange costs [$]
Lévy-flight MFOA	**17.5**	**30**	**41**	**9**	**–173,344**
MFOA	17.5	30	44	12	–175,919
GA	17.5	30	48	12	–177,354
Hybrid GA-PSO	17.5	30	48	12	–176,960
PSO	17.5	30	48	12	–187,899
ALO	12.5	35	50	15	–311,679
HS	7.5	40	51	15	–315,899
SA	7.5	40	51	15	–316,099
ABC	7.5	40	51	15	–318,064
ACO	2.5	45	52	15	–319,735

*Bold indicates the least-cost mix of the decision variables obtained across the examined meta-heuristics over 30 independent simulation runs.

comparative analysis because none of the algorithms reached the physical limits to how much computation can be executed during the planning phase of MGs in real-world settings. The developed meta-heuristic efficiency comparison framework involves two stages: First, the meta-heuristics are scored locally with respect to each criterion (according to the calculated descriptive statistics). The scores for the selected criteria are then averaged in the second stage to yield the final rank order of the analysed meta-heuristics. The summary statistics for the comparative efficiency of the examined meta-heuristics are revealing in the following ways:

- Based on the descriptive statistics, the following overall efficiency ranking can be produced in the context of optimal MG sizing: the Lévy-flight MFOA > the MFOA > the GA > the HGA-PSO > the PSO > the ALO > the HS > the SA > the ABC > the ACO. While the examined meta-heuristics have yielded somewhat different rankings across different indicators, the Lévy-flight MFOA has consistently ranked first in terms of all of the individual indicators. This statistically robust evidence indicates that the Lévy-flight MFOA is an ideal choice for meta-heuristic-based MG capacity planning optimisation.
- Integrating Lévy flights into the search process of the MFOA is able to improve the trade-off between the exploration and exploitation phases, which results in more effective long-range jumps around the global search space and an efficient local search near the global optima. Accordingly, the quality of the solution optimised by the Lévy-flight MFOA is higher than that of the original MFOA by a significant ~6.5% in the best run, and by as much as ~7.3%, on average. This suggests that approximately two-thirds of the expected cost savings (~11.5% in the best run), when measured against the solution optimised by the HOMER Pro software, are attributable to the modelling feature of optimising the strategic MG investment planning and the day-ahead energy scheduling problems in an integrated way.
- The comparative statistical results are consistent with previous findings in the literature on the outperformance of the original MFOA to the well-established and state-of-the-art meta-heuristics in economic MG planning applications [53–55]. Moreover, the GA, the hybrid GA-PSO, and the PSO are ranked 3 to 5, respectively, which explains their popularity in the mainstream MG capacity planning optimisation literature [4–10].
- A comparison of the solutions optimised by the Lévy-flight MFOA and the ACO in their best performance trials indicates that failure to employ a fitting optimisation algorithm, while optimally designing a MG system using meta-heuristics, could potentially result in an overestimation of its lifetime cost by at least ~13%. This translates into an extra cost of ~$6k for the case under study over its lifetime. However, this may not imply a significant saving from a practical point of view, which is due to the relatively small scale of the case study. That is, the outperformance of the Lévy-flight MFOA over the investigated meta-heuristics is more substantial when applied to more structurally complex MGs of utility-scale.
- The root-mean-square error of the population of the MG whole-life costs returned by the proposed Lévy-flight MFOA-optimised model over the 30 trials with respect to its best performance was found to be negligible (~0.4%). This indicates the robustness of the proposed model to the random initialisation process, which, in turn, suggests the adequacy of a single run of the algorithm.

Moreover, Table 7 provides a breakdown of the optimal combination of the decision variables optimised by the selected meta-heuristics in their best runs. The table is revealing in several important ways:

- The Lévy-flight MFOA, the basic MFOA, the GA, the PSO, and the hybrid GA-PSO agree on the optimal combination of the sizes of the solar PV and WT generation systems. That is, the difference in the efficiency of these algorithms arises from a difference in the optimised sizes of the battery bank and the multi-mode inverter, which consequently alter the energy trading capacity of the MG with the utility grid. More specifically, in all of these cases, the obtained reductions in the total net electricity exchange costs were not sufficient to offset the increased costs associated with the respective increased sizes of the battery and inverter. Further analyses revealed that the reductions in the total net electricity exchange costs – the sum of the hourly grid import costs minus hourly grid export revenues over the project life-cycle – are, in large part, attributable to reductions in grid import costs, rather than increases in grid export revenues. This observation can be explained by the unaltered sizes of the distributed generation technologies; the larger battery bank capacity allows storing extra energy for later use, which can be translated into less imports during higher-priced peak periods.
- The GA, the PSO, and the hybrid GA-PSO yield exactly the same set of cost-optimal sizes for the technologies considered in the candidate pool; the difference in the MG life-cycle costs estimated by these algorithms is solely associated with the expected total net energy purchased with direct influence on the total net electricity exchange costs. Similar observations held true for the ABC, the SA, and the HS algorithms. It is also worth noting that no meta-heuristic yielded a battery-less MG configuration in the optimised mix of technologies.
- All the examined meta-heuristic optimisation algorithms agree that the optimal total renewable energy generation capacity is equal to the active power rating of the existing installed transformer at the site. However, four different combinations of the sizes of the solar PV and WT plants (with different battery storage and inverter capacities) were observed across the best solutions returned by the selected

figuration were observed in light of the single cost-minimisation objective considered, it was decided to limit the statistical analyses to the resulting total discounted system costs.

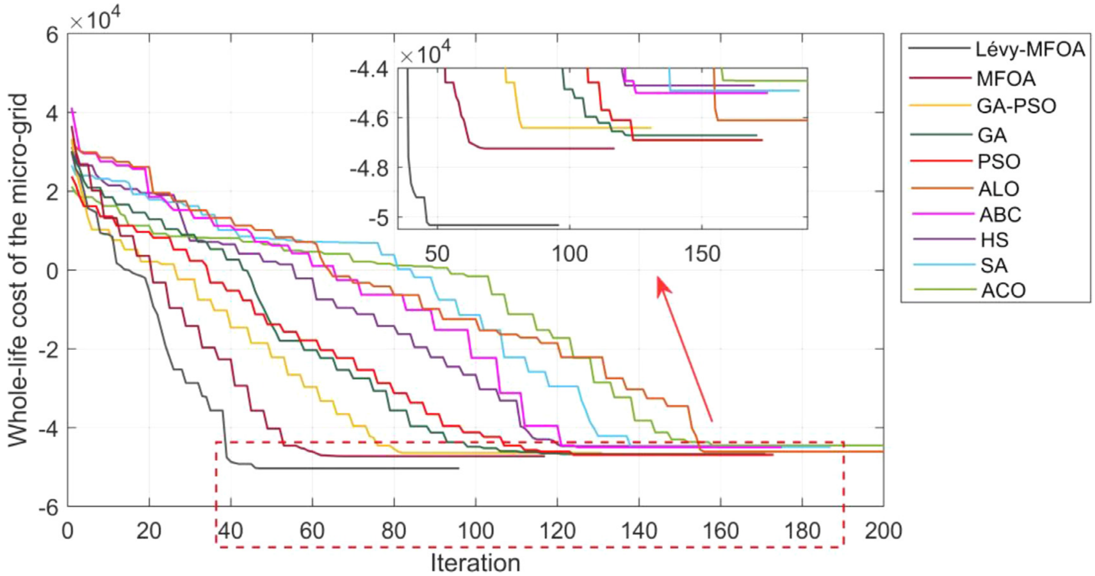

Fig. 15. Convergence patterns of the selected meta-heuristics in their best runs.

meta-heuristic optimisers. The more the combinations of the sizes of the two generation technologies deviate from the point with 17.5 kW solar PV and 30 kW WT, the worse the MG whole-life cost solution.

Additionally, Fig. 15 shows the convergence process of the selected optimisers in their best trials. The figure demonstrates the adequacy of the selected values for the stopping criteria, whilst additionally indicating the comparatively fast convergence of the Lévy-flight MFOA and the basic MFOA in terms of the number of iterations. Recall that the imposed adaptive stopping criterion – which terminates the search procedure after 50 successive calls with no improvement in the best solution – addresses both the early stopping and late stopping issues.

As its superiority to the other meta-heuristics studied is shown to be statistically valid, the modelling results presented hereafter are based on the best-performing trial of the Lévy-flight MFOA (with the corresponding whole-life cost and values of the decision variables highlighted in bold in Tables 6 and 7).

4.3. Energy balance analysis

This section presents a monthly resolved overview of the balance of energy generation/imports and consumption/exports/dissipation, as well as two indicative hourly-basis, one-day energy balance analyses.[8] The analyses were made based on the least-cost energy mix solution estimated by the best run of the proposed Lévy-flight MFOA-based solution approach integrating the day-ahead scheduling design framework. Fig. 16 summarises the monthly energy generation/imports and consumption/exports/dissipation over the representative year. The resulting values are based on a one-year operational period with hourly intervals under the energy reliability and resilience constraints of $LPSP^{max} = 0$ and $SSR^{min} = 80\%$, respectively.

As Fig. 16 shows, the ratio of monthly resolved solar PV-to-wind generation data undergoes statistically significant changes throughout the year. Specifically, the ratio is highest during the summer period between December and February (at around 42%, on average) and lowest during the winter period between June and August (at around 18%, on average). The yearly breakdown of the on-site renewable power generation indicates around 20,382 kWh (~21%) of solar PV energy generation and 78,891 kWh (~79%) of wind energy generation per year, on average. The self-sufficiency ratio of the optimal system was found to be 80% (i.e., the minimum allowed value), which indicates that 20% of the total yearly load demand on the MG is met through imports.

On the other hand, as planned, a substantial fraction of the year-round electricity generated by renewables (~71%) is sold back to the grid as 'net excess generation', followed by the local energy consumption (~23%). The remainder of the year-round renewable energy generation, totalling 5,957 kWh (~6%), is lost during the power and energy conversion processes, with the breakdown of the contributors as follows: transformer, ~48%; hybrid inverter, ~33%; and the battery bank, ~19%.[9]

Additionally, Fig. 16 gives further credence to the observation that the battery bank contributes significantly to cost reduction and efficiency improvement. Notably, further analyses identified that a significant ~76% of the total annual load demand is managed by the battery bank – as measured by the yearly average ratio of battery discharging power to power load. As it can be inferred from a comparison of the actual battery capacity used over different seasons in Fig. 16, much of the battery bank-integrated system's success is due to its ability to flatten the net demand in peak winter season, leading to a full (available) resource adequacy credit by protecting the MG from higher wholesale market prices.

To further validate the reliable operation of the Lévy-flight MFOA-optimised MG system that benefits from the day-ahead linear-programming-based scheduling framework, Fig. 17 provides representative hourly-basis, one-day energy balance analyses for the minimum and maximum 'net' system demand days, namely February 3rd and July 17th, respectively. See the Supplementary Material accompanying the paper for raw data (Additional File 1: Tables S1 and S2).

As Fig. 17 shows, during the first 5 hours of the minimum net system demand day (light load hours), the on-site renewable power generation is entirely stored in the battery bank, while the load demand is met solely through low-cost grid imports. This observation can be explained by the intelligent scheduling design's foresight to realise that there will be a

[8] Note that given the considered 100% energy dispatch reliability constraint and the zero curtailed electricity achieved, the total energy supplied by the renewable energy resources is equal to the sum of the total energy demand on the system, the total net energy exported to the upstream grid, the total net battery charging power, and the total power loss due to conversion – on any given time scale.

[9] The efficiency of the existing installed transformer and multi-mode inverter were respectively assumed to be 94% (round-trip) and 96%, while the charging and discharging efficiencies of the battery packs were assumed to be 92%.

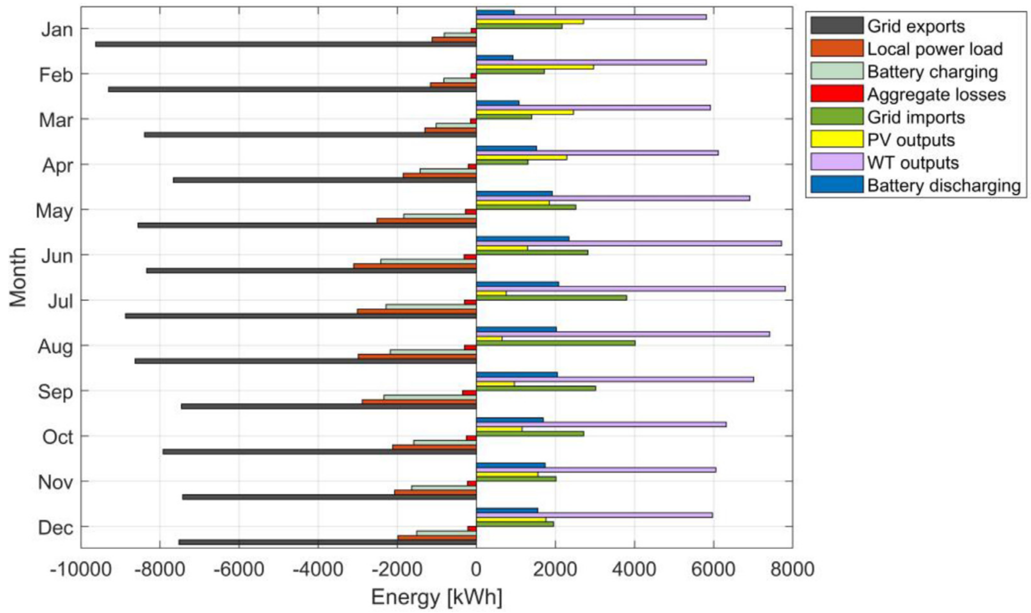

Fig. 16. Monthly energy balance analysis of the MG over the baseline operating year. A positive (negative) value represents the inflow (outflow) of energy to (from) the busbars of the MG system.

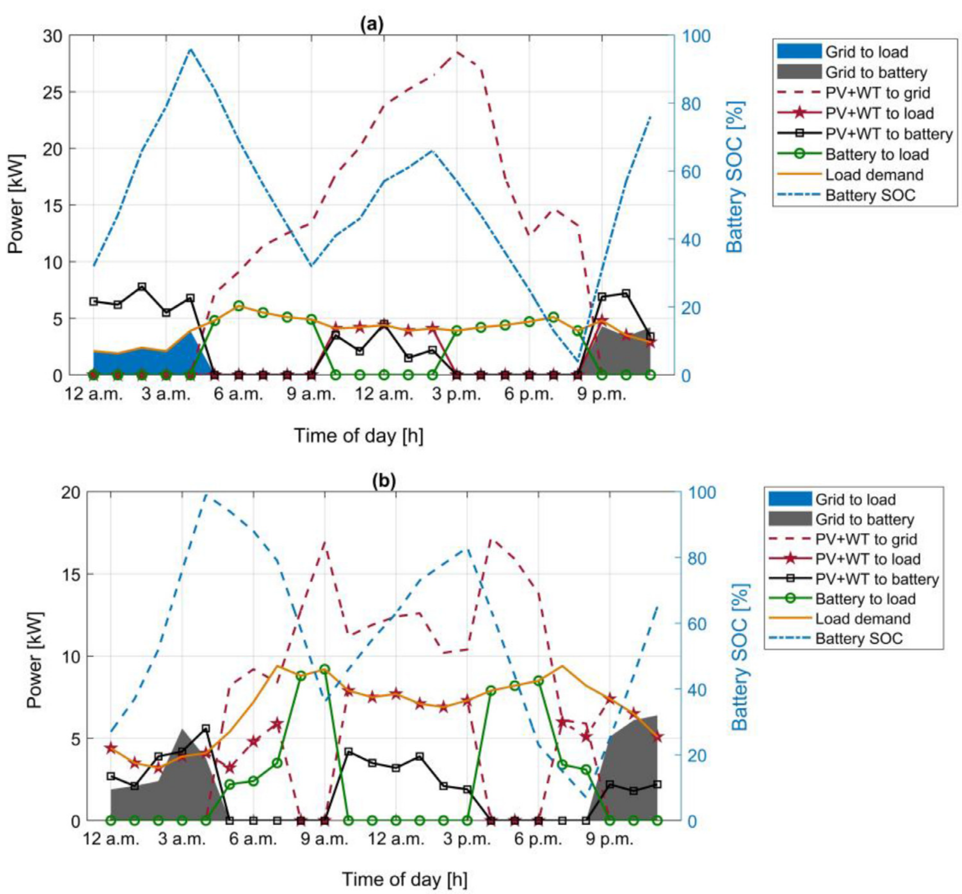

Fig. 17. Hourly-basis, one-day operating analysis of the MG system: (a) the minimum net system demand day; (b) the maximum net system demand day. Note the change in scale in the dependent axes.

significant rise in the wholesale electricity market price during the day-specific morning peak period in terms of 'net' demand (5 a.m. through 9 a.m.), where the cost-optimal operational strategy is to sell the entire renewable power generation back into the grid and meet the local load totally by discharging the storage system. Then, from hour 10 a.m. to 2 p.m., any excess renewable energy is optimally decomposed into the battery charging power (to gradually replenish its energy content for the upcoming evening peak period) and grid exports, whilst adhering to the battery charge power capacity and the existing installed transformer capacity. This is because the look-ahead energy dispatch strategy is able to predict that both the demand and wholesale prices will significantly rise at around 3 p.m. Then, during the day-specific evening peak hours (3 p.m. to 8 p.m.), the on-site non-dispatchable renewable power generation is entirely exported to the upstream grid, while releasing the energy in store meets the power loads (note the equality of the battery discharging power and load power). Finally, notwithstanding the fact that the operational scheduling design lacks any foresight of demand, generation, and wholesale prices beyond the current 24-h scheduling horizon, the battery bank is interestingly charged jointly by the excess renewable energy generation and grid imports during the late evening period (9 p.m. to 11 p.m.). The reason behind importing electricity from the grid to more sharply charge the battery bank during the last hours of the 24-h scheduling horizon is to cost-optimally relax the terminal constraint on the battery energy content at the end of the one-year analysis period (see Eq. (10)). Recall that the battery bank cannot be simultaneously charged and discharged, and power imports and exports cannot occur at the same time.

In contrary to the early morning hours of the minimum net system demand day (where grid imports meet the demand while the entire renewable power generation is directed to charging the battery bank), during the first 5 hours of the maximum net system demand day, the load demand is served solely by the wind power, the excess of which charges the battery bank in addition to grid imports (to reach a battery SOC of ~100%). There are at least three reasons for the observed difference in the operational strategy (increased grid imports during the early morning hours) compared to the minimum net system demand day for the relevant period, namely: (1) lower wholesale prices, (2) higher power loads in the upcoming morning peak period, and (3) lower on-site renewable generation during the day due to minimal solar radiation in the wintertime. Accordingly, the cost-optimal schedule in the morning peak period is to meet the power loads by an optimal mix of renewable generation and battery discharging power from hour 5 a.m. to 7 a.m. to be able to make the most profit possible from grid exports in the next two higher-priced hours of the day-specific morning peak period (8 a.m. and 9 a.m.) where loads are served solely by the battery discharging power. Then, likewise to the corresponding shoulder-peak hours of the minimum net system demand day, any excess renewable energy generation is optimally allocated to grid exports and battery charging. The goal is to reach a battery SOC level at the end of the shoulder-peak period (3 p.m.) that is sufficient to meet the loads solely by drawing energy from the battery bank during the higher-priced day-specific evening peak hours (4 p.m. to 6 p.m.), while the battery charging rate depends on the hourly forecasts of wholesale prices. Also, during the relatively lower-priced evening peak hours (7 p.m. and 8 p.m.), the power loads are satisfied by an optimal mix of battery discharging power and on-site renewable power generation, the remainder of which is exported to the grid. Finally, with the depletion of the battery bank, from hour 9 p.m. to midnight, the battery bank is charged from grid imports and excess wind power simultaneously. It should also be noted that the load demand served directly by the utility grid amounts to zero in the entire maximum net system demand day.

As the above discussion on the daily energy management of the cost-optimal MG design indicates, the battery energy storage system plays a key economic role in the operation of the grid-connected MG system by an indirect arbitrage shifting renewable energy output – battery charging during less valuable and costly times of day by excess renewable power and grid imports, respectively, and battery discharging to serve the local demand during more remunerative times of day (with respect to the wholesale electricity market prices), enabling increased energy exports.

4.4. Cash flow analysis

The optimal total net present cost of the system is found to be −$50,332, which is composed of the equipment-related and power exchange-related cost components, which are found to be $123,012 and −$173,344, respectively. That is, energy trading with the grid is highly profitable, making an estimated $2,517 of yearly profit. Note that the profits are derived, in large part, from selling the excess wind power, as the WT generation system capacity is optimised to be significantly larger than what is required to cost-effectively meet the local demand. This can be justified by the calculated payback period of the turbines (approximately 6.5 years), which is considerably lower than their expected lifetimes (20 years) when used solely for grid export purposes. However, it should be noted that it is assumed that network constraints do not block the acquisition of resources into the wholesale market, whilst additionally network charges and service fees collected by the FRMP were not taken into account.

The equipment-related financial component can be further broken down into the following subcomponents: total capital cost, $109,172; total replacement cost, $28,875; total O&M cost, $6,621, and total salvage value, −$21,656. Fig. 18 provides a further breakdown of the MG's total net present worth by the underlying equipment-related financial subcomponents. As it can be seen from the figure, the PV generation system, WTs, battery packs, and inverters comprise about 18%, 34%, 34%, and 14% of the total equipment-related net present cost of the MG system, respectively.

Moreover, Fig. 19 provides an overview of the cumulative discounted cash flow analysis over the MG life-cycle period. As the figure shows, a relatively significant capital outlay is expected, in addition to the battery and inverter replacement costs in Year 15 of the project, as well as annual O&M and grid import costs. On the other hand, the sources of cash inflow include the power sold to the customers (at a flat rate of $0.23/kWh, in compliance with the most recent average domestic electricity price at the studied site [102]) and the power exported back to the grid (traded at the dynamic forecasts of spot electricity market prices shown in Fig. 10(e)). Recall that it is assumed that a retail intermediary provides access to the wholesale electricity market.[10] The figure also indicates that the entire $123,012 investment, if realised, would be recouped within around 10 years.

4.5. Capital budgeting analysis

To aid the associated capital planning decision-making process, this section provides a cost-benefit analysis using three key financial appraisal metrics in the MG investment planning context, namely: the levelised cost of energy (LCOE), the modified internal rate of return (MIRR), and the discounted profitability index (DPI).

4.5.1. Levelised cost of energy

The LCOE of an energy system is defined as the discounted total lifetime costs it incurs divided by its discounted total lifetime energy outputs. For a grid-connected solar PV/WT MG system planned to serve the local demand with 100% reliability over its life-cycle, the LCOE can be mathematically formulated as [103]:

$$LCOE = \frac{\sum_{c \in C} NPC_c + NPC_{tr,net}}{\sum_{n=1}^{PL} \frac{\sum_{t=1}^{8760} (P_{PV}(t) + P_{WT}(t))}{(1+ir)^n}}. \tag{39}$$

4.5.2. Modified internal rate of return

While the normal internal rate of return (IRR) indicator is widely adopted in the MG planning literature to measure the profitability of a project, it has a fundamental shortcoming: it (impractically) assumes the reinvestment to take place at the IRR, which could lead to overly optimistic projections and, consequently, capital budgeting mistakes. Furthermore, the IRR indicator is not applicable to the projects where the intermediate cash flows are not going to be reinvested. However, the MIRR provides project managers with direct control over the assumed reinvestment rate from future cash flows [104,105]. In this light, the MIRR can be adapted for application in the context of MG planning as

[10] For example, under the 'Home Harvest' programme of the Flick Electric CO in New Zealand. For more details, see: https://www.flickelectric.co.nz/home-harvest [Accessed: 11-Nov.-2020].

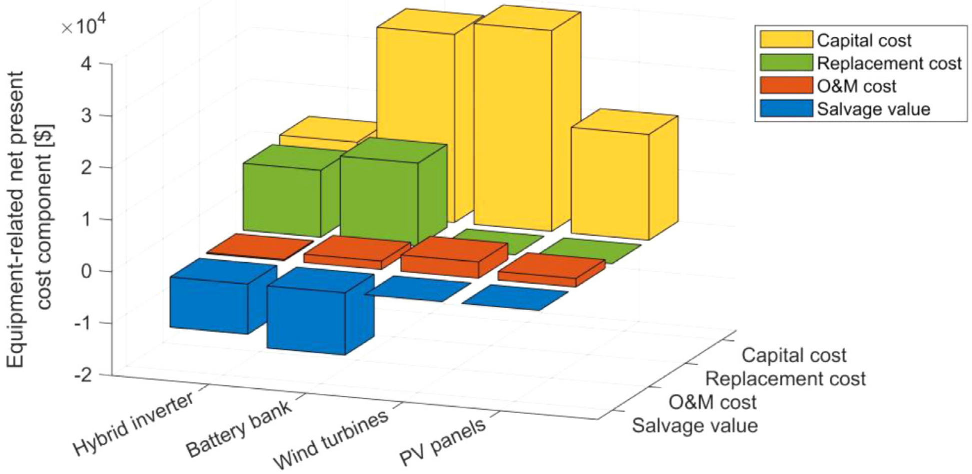

Fig. 18. Breakdown of the MG lifetime cost by the equipment-related cost subcomponents.

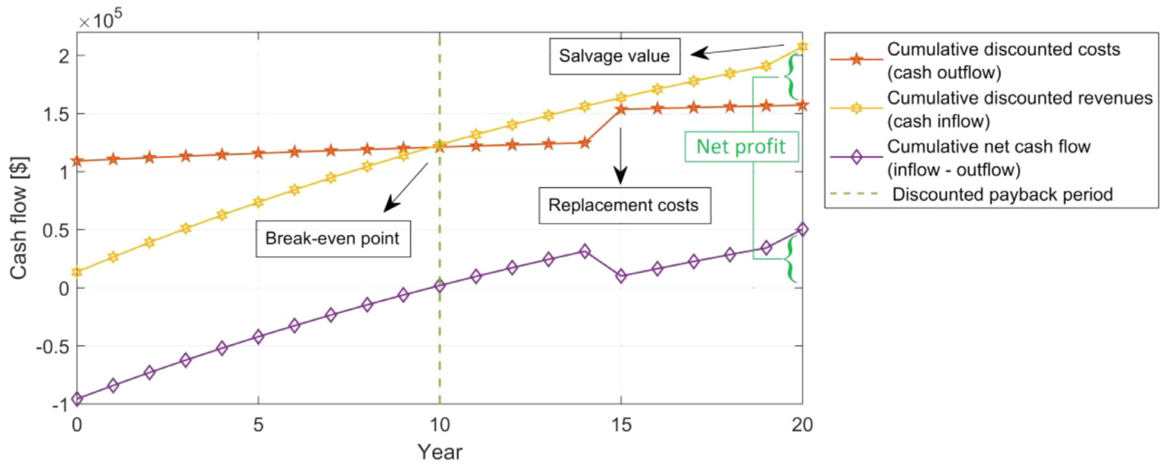

Fig. 19. Discounted break-even analysis over the life-cycle of the project.

follows [106]:

$$MIRR = \sqrt[PL-1]{\frac{\sum_{n=1}^{PL} R(n) \times (1+RR)^{PL-n}}{\left|\sum_{n=1}^{PL} \frac{WLC_{ann}(n)}{(1+ir)^{n-1}}\right|}} - 1, \quad (40)$$

where $R(n)$ is the total revenue generated by providing energy services and power exports in year n, $WLC_{ann}(n)$ denotes the annualised WLC_{MG}, which can be calculated by multiplying the whole-life cost of the system by the relevant capital recovery factor (see Eq. (5)), and RR represents the reinvestment rate, which is assumed to be 0% in this paper.

4.5.3. Discounted profitability index

The profitability index (PI), alternatively referred to as value investment ratio or profit investment ratio, measures the present value of future cash flows relative to the capital investment. The DPI is a modified variant of the PI, which factors in the time value of money. Accordingly, the DPI of the modelled MG system can be determined by the following equation [107,108]:

$$DPI = \frac{\left|PV(TRC + TO\&M - TSV) + TNPC_{tr,net}\right|}{TCC}, \quad (41)$$

where TCC denotes the total capital cost of the MG assets, TRC, $TO\&M$, and TSV represent the total discounted replacement cost, O&M cost, and salvage value of the energy infrastructure, $TNPC_{tr,net}$ identifies the total net present cost associated with power trading with the grid over the MG lifetime, with $PV(\cdot)$ denoting the present value function.

Any DPI value lower than 1.0 is undesirable, as it indicates that the present value of the project is lower than the capital outlay. As the value of DPI increases above 1.0, the financial attractiveness of the proposed design does so as well [109].

4.5.4. Resulting capital budgeting metrics

The LCOE, MIRR, and DPI of the investment proposal were respectively found to be −\$0.02/kWh, 5.4%, and 1.43. The resulting metrics for the cost-optimal conceptual MG configuration were compared to those obtained for a baseline case scenario. The base case scenario represents the site's existing electricity supply system. Currently, the site has an installed solar PV capacity of 11.4 kW_p; the current practice is to feed any excess renewable power back into the grid during the day (at the existing feed-in-tariff rate of \$0.08/kWh) and to import electricity from the grid at night when the solar system does not generate. The electricity is purchased at the retailer-determined flat-rate electricity tariff of \$0.23/kWh. Table 8 compares the resulting capital budgeting metrics for the two scenarios. Specifically, the resulting indicators for the proposed MG configuration represent the system optimised by the proposed Lévy-flight MFOA-based MG sizing model with an integrated LP-based operational strategy. Furthermore, the capital budgeting metrics for the fixed-sized PV-only system were calculated by operating the system based on the optimisation-based forward-looking operational strat-

Table 8
Comparative summary of the capital budgeting analysis for the proposed and existing electricity supply systems.

System	Capital budgeting metric LCOE[a]	MIRR	DPI
PV-only system (including solar inverters)	\$0.39/kWh	2.2%	1.09[b]
Proposed PV/WT/battery MG	−\$0.02/kWh (−105%)	5.4% (+145%)	1.43 (+31%)

[a] Mathematically, the LCOE becomes negative when the present worth of the net cash flows in Years 1 and later of the project are more positive than the Year 0 cost is negative – or, put differently, when the projected total out-year benefits (generated from grid exports, local power sales, and equipment salvage value) are higher than the sum of the costs of initial investment, equipment replacement, system O&M, and grid imports.

[b] Since making the considered site highly energy self-sufficient did not form part of the PV-only scheme's objective, the net cash flows associated with the energy exchanged with the grid included only the savings from not having to buy electricity from the grid during daytime and any income generated from grid exports – both of which were treated as cash inflows. That is, the costs of power imports were excluded from the calculation of the relevant metrics for the sake of a fair comparison.

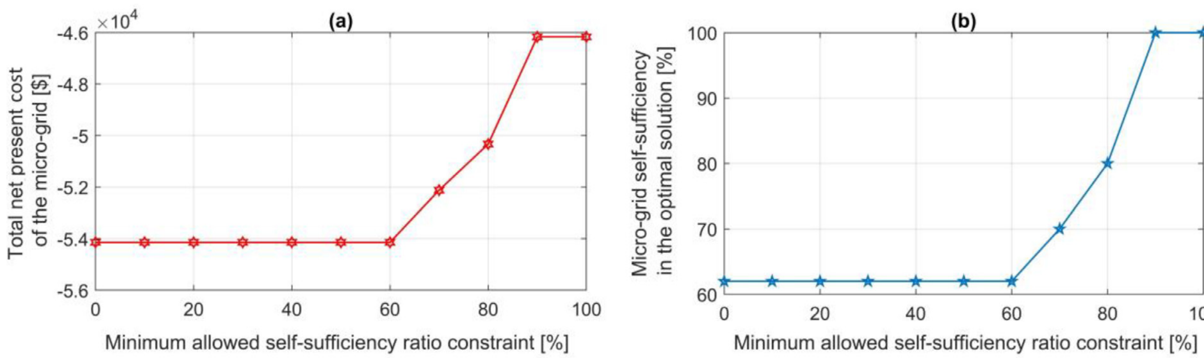

Fig. 20. Sensitivity analysis with respect to the minimum allowed self-sufficiency ratio: (a) the MG whole-life cost; (b) the optimal self-sufficiency ratio.

egy for a representative year (over a moving 24-hour time window), and then computing a series of annual net financial flows adjusted for the discount rate. Note that the percentages in the table refer to the deviation of the obtained budgeting metrics for the proposed system from those obtained for the PV-only scenario. It should also be noted that to level the playing field, the solar PV-only scenario was assumed to begin operation at the same time as the proposed MG system and the same brands of solar PV panels and inverters were considered.

The comparative capital budgeting analysis of the existing and proposed electricity supply systems based on the selected financial appraisal metrics reveals that the proposed community MG project is a low-risk, high-return investment opportunity suitable for community ownership. More specifically, the comparably low MIRR value calculated for the PV-only investment scenario and the corresponding value of the DPI that is only slightly above one collectively reveal that the current practice does not yield an adequate return on investment. Additionally, if the costs associated with grid imports were factored into the capital budgeting analysis for the PV-only system, the total costs would outweigh the benefits and the project would be expected to result in a net loss. By contrast, the resulting metrics for the conceptual MG indicate that the project proposal is able to readily attract third-party investment from energy service companies, or any other private investor while guaranteeing a steady revenue stream.

4.6. Sensitivity analysis: economics of self-sufficiency

A sensitivity analysis is provided in this section to understand the robustness of the whole-life cost of the system to changes in the minimum allowed self-sufficiency ratio, which is treated as a bounded constraint. To this end, the optimisation process was repeated for multiple values of the minimum self-sufficiency ratio ranging from 0% to 100% in intervals of 10%, totalling 11 optimisation cases. Fig. 20 depicts the sensitivity of the total discounted system costs and the optimal system self-sufficiency with respect to changes in the value of the imposed minimum allowed self-sufficiency ratio constraint. The following key observations can be made from the figure:

- Imposing different values for the minimum allowed self-sufficiency ratio does not significantly alter the MG whole-life cost results. The percentage error between the MG net present worth solutions under 0% and 100% minimum allowed self-sufficiency ratio constraints is as low as 14% (equating to ∼\$8k). Interestingly, further analyses indicated that the changes in the size of the battery bank and the total power exchanged with the grid were the only contributors to the differences observed in the total discounted system costs. More specifically, in both scenarios, the optimal mix of the non-dispatchable power generation components were found to include 17.5 kW of solar PV arrays and 30 kW of WTs. Furthermore, the optimal capacity of the battery bank was found to be 38 kWh and 43 kWh respectively in the lower and upper extreme cases.
- Solving the model instances with the minimum allowed self-sufficiency ratio values ranging from 0% to 60% yields the same least-cost solution. The underlying reason for this is that the optimal solution returns an actual self-sufficiency ratio of approximately 62% in the case with SSR^{min} = 0%, where practically no minimum self-sufficiency constraint is active.
- The resulting MG whole-life costs obtained for the cases in between the cases with SSR^{min} = 60% and SSR^{min} =100% suggest that there are important dynamics that are taking place with the corresponding constraint. Specifically, the optimal value of the self-sufficiency ratio of the system was found to be 70% and 80% in the cases with SSR^{min} = 70% and SSR^{min} = 80%. A comparison of the MG net present values obtained under the above two scenarios indicates a linear cost increase to meet the prescribed minimum

self-sufficiency ratios – which can be referred to as a “relative cost of self-sufficiency”. However, the actual self-sufficiency ratio of the case with the imposed constraint of $SSR^{min} = 90\%$ was found to be 100%. This can be explained by the fact that the problem is optimised over a discrete search space in that the step size for the battery bank capacity is 1 kWh. Accordingly, a redundant 0.7 kWh battery capacity increment that is unnecessary for meeting the 90% self-sufficiency target – but unavoidable due to the limited resolution of the battery size step length – makes the 100% self-sufficiency scenario the cost-optimal choice.

5. Conclusions and future work

This paper has presented a novel Lévy-flight MFOA-based solution approach to determining the cost-minimal future generation/storage/conversion technology mix for a given electrical demand, whilst additionally optimising the operational strategy of the system using a LP-based technique over a 24-h moving horizon. The model addresses key methodological gaps in the meta-heuristic-based MG capacity planning approaches present in the literature, as well as renewable energy system modelling software tools available commercially – that seek to derive a simplified closed-form solution to the energy planning optimisation problem. The application of the model to the numerical test case of a rural subdivision in New Zealand that has a connection to the main grid, and the comparison of the optimisation results of the Lévy-flight MFOA with those of the most widely-used and most promising meta-heuristics in the literature, as well as the industry-leading MG modelling software, HOMER Pro, led to several key observations and, in turn, generated novel methodological insights, namely:

- Significant differences between the cost-optimal solutions produced by the proposed meta-heuristic-based model and the HOMER Pro software were observed both in terms of system architecture and total discounted system costs. Specifically, a ~18% underestimation of the total net present worth of the project by HOMER Pro was shown. This challenges the accuracy of the optimisation algorithms embedded in the existing MG sizing tools.
- In contrast to the HOMER Pro model, the energy infrastructure mix optimised by the proposed model includes a stationary Li-ion battery bank, which significantly contributes to cost reduction and efficiency. This is mainly driven by optimising the MG dispatch over a moving 24-hour horizon – a feature that is not found in the mainstream software packages tailored to MG capacity planning.
- While all the tested meta-heuristics yielded the same optimal system configuration, the Lévy-flight MFOA was able to find a solution set (including the sizes of the components and the total power exchanged with the utility grid) that returns a comparably lower total discounted system cost. Specifically, it indicated the problem’s optimal net present worth to be higher than those estimated by the original MFOA, the PSO, the GA, the hybrid GA-PSO, the ALO, the ABC, the SA, the HS, and the ACO – in their corresponding best runs throughout 30 trials – by at least 6.5%, 7.3%, 7.7%, 8.4%, 9.1%, 11.8%, 12.1%, 12.6%, and 12.9%, respectively. Further comparative analyses revealed that much of the differences in the modelling solutions was attributable to the estimated potential for energy exchange with the upstream grid.
- When nested within the meta-heuristic design optimisation of MGs, the day-ahead operational planning optimisation is able to produce cost-savings of at least 11.5% through adding strategic foresight to the integrated energy planning decision-making process in terms of future wholesale prices, load demand, and renewable generation.
- Solving the MG sizing problem using meta-heuristics is computationally demanding as it involves determining the year-long, hourly-basis energy balance of the infrastructure mix selected by each of the hundreds of the meta-heuristic of interest’s search agents. However, since the MG investment planning is a one-time optimisation exercise, the running time limits are exceptionally high within the renewable energy system optimisation context.

The econometric and case study analyses evidenced the effectiveness of the proposed Lévy-flight MFOA-optimised integrated operational and investment planning approach in producing significant percentage points of cost-savings at a residential subdivision scale. However, the *actual differences* between the net present values returned by the proposed model and the HOMER Pro software and, more debatably, between the results yielded by the model instances optimised by different meta-heuristic optimisation algorithms, were not as marked; at around $9,000 (at most) due to the size of the case study. This implies that the superiority of the proposed MG capacity planning modelling framework is more pronounced for larger-scale systems. Further work should, therefore, quantify the effectiveness of the devised model for the co-optimisation of the design and operation of MGs when applied to large-scale community projects.

Furthermore, in-depth energy management analyses for the minimum and maximum net system demand days have substantiated the feasibility and stability of the resulting MG designs. Capital budgeting analyses have also demonstrated the economic superiority of the project proposal to the studied site’s existing solar PV/grid electricity supply system. In terms of economics, it has additionally been found that it is not infeasible for the inhabitants to have the financial clout to be able to own the conceptual system outright, though it also can be readily financed through third-party ownership options (such as power purchase and lease agreements) – as it represents an attractive investment opportunity. Moreover, a sensitivity analysis of the MG whole-life cost with respect to the minimum self-sufficiency ratio failed to identify any substantial impact of the self-sufficiency constraint on the total discounted system costs: Forcing a minimum self-sufficiency ratio of 100% increases the MG lifetime costs by only 14% compared to the case where no self-sufficiency constraint is imposed. The reason lies in the surpassed grid parity, which has significantly contributed to increasing the adequacy margins of the simulated system. However, the costs associated with the transformer capacity, network charges, and service fees collected by the third-party aggregator (enabling access to the wholesale market) were not factored into the techno-economic analysis – and the grid exchanges were bounded by the site’s existing installed transformer capacity. That is, exploring the grid parity of the system while incorporating such sources of additional cost represents another interesting area for future research.

In addition, the solutions estimated by the selected meta-heuristics are ranked from a pure cost optimisation perspective. That is, the findings on the rank order of the examined meta-heuristics might not be generalisable to their multi-objective variants. Accordingly, research is needed to explore the efficiency of the multi-objective variants of the selected algorithms when applied to multi-criteria renewable energy system planning optimisation. In this light, one interesting objective that could be maximised in conjunction with minimising the system whole-life cost is the battery bank autonomy – as an energy resilience criterion.

Moreover, in this paper, all parametric inputs are assumed deterministic, which presents another limitation to the model in terms of handling the model-inherent parametric uncertainties. Future work will add a probabilistic uncertainty quantification dimension to the model to better reflect reality and support decision-making during the energy infrastructure planning process.

Declaration of Competing Interest

The authors declare that they have no known competing financial interests or personal relationships that could have appeared to influence the work reported in this paper.

CRediT authorship contribution statement

Soheil Mohseni: Conceptualization, Methodology, Data curation, Formal analysis, Investigation, Resources, Software, Validation, Visualization, Writing - original draft. **Alan C. Brent:** Supervision, Project administration, Formal analysis, Investigation, Resources, Validation, Writing - review & editing. **Daniel Burmester:** Supervision, Formal analysis, Investigation, Validation. **Will N. Browne:** Supervision, Formal analysis, Investigation, Validation.

Acknowledgments

The authors would like to gratefully acknowledge suggestions and contextual input provided by the Totarabank Subdivision developer Andy Duncan.

Supplementary materials

Supplementary material associated with this article can be found, in the online version, at doi:10.1016/j.egyai.2021.100047.

Appendix A. Loss of power supply probability

The loss of power supply probability is an indicator of the reliability of power supply, which is defined as the sum of the shortages of power generation capacity divided by the total power demand on the system over the operation analysis period, which can be expressed as follows [74]:

$$LPSP = \frac{\sum_{t=1}^{T} (LPS(t) \times \Delta t)}{\sum_{t=1}^{T} (P_{dem}(t) \times \Delta t)}, \quad \text{(A.1)}$$

where $LPS(t)$ is the loss of power supply at time-step t when demand outstrips supply, as defined in Eq. (A.2), $P_{dem}(t)$ is the load power demand at time-step t, Δt is the duration of each time-step, and T is the length of the operating horizon.

$$LPS(t) = \begin{cases} P_{dem}(t) - P_{sup}(t) \ \mathit{if} \ P_{dem}(t) > P_{sup}(t), \\ 0 \quad \mathit{otherwise}, \end{cases} \quad \text{(A.2)}$$

where $P_{sup}(t)$ denotes the total power supplied by the on-site distributed energy resources (i.e., the generation and storage equipment) at time-step t of the system operation over the operating horizon T.

In the grid-connected renewable energy system context, P_{sup} includes the power imported from the upstream grid, in addition to the power generated by the on-site distributed energy resources. It is also worth noting that in the context of long-term renewable energy system investment planning, T is often set to 8,760 hours (i.e., a one-year simulation study) and the duration of each time-step is often taken equal to 1 hour.

References

[1] Hiremath RB, Shikha S, Ravindranath NH. Decentralized energy planning; modeling and application—a review. Renew Sustain Energy Rev 2007;11(5):729–52.
[2] Trotter PA, Cooper NJ, Wilson PR. A multi-criteria, long-term energy planning optimisation model with integrated on-grid and off-grid electrification–the case of Uganda. Appl Energy 2019;243:288–312.
[3] Mohseni S, Moghaddas-Tafreshi SM. A multi-agent system for optimal sizing of a cooperative self-sustainable multi-carrier microgrid. Sustain Cities Soc 2018;38:452–65.
[4] Gamarra C, Guerrero JM. Computational optimization techniques applied to microgrids planning: a review. Renew Sustain Energy Rev 2015;48:413–24.
[5] Fathima AH, Palanisamy K. Optimization in microgrids with hybrid energy systems - a review. Renew Sustain Energy Rev 2015;45:431–46.
[6] Emad D, El-Hameed MA, Yousef MT, El-Fergany AA. Computational methods for optimal planning of hybrid renewable microgrids: a comprehensive review and challenges. Arch Comput Methods Eng 2020;27:1297–319.
[7] Sinha S, Chandel SS. Review of recent trends in optimization techniques for solar photovoltaic-wind based hybrid energy systems. Renew Sustain Energy Rev 2015;50:755–69.
[8] Hannan MA, Faisal M, Jern Ker P, Begum RA, Dong ZY, Zhang C. Review of optimal methods and algorithms for sizing energy storage systems to achieve decarbonization in microgrid applications. Renew Sustain Energy Rev 2020;131:110022.
[9] Yang Y, Bremner S, Menictas C, Kay M. Battery energy storage system size determination in renewable energy systems: a review. Renew Sustain Energy Rev 2018;91:109–25.
[10] Mellit A, Kalogirou SA. MPPT-based artificial intelligence techniques for photovoltaic systems and its implementation into field programmable gate array chips: Review of current status and future perspectives. Energy 2014;70:1–21.
[11] Chen Q, Xia M, Zhou Y, Cai H, Wu J, Zhang H. Optimal planning for partially self-sufficient microgrid with limited annual electricity exchange with distribution grid. IEEE Access 2019;7:123505–20.
[12] Al-falahi MDA, Jayasinghe SDG, Enshaei H. A review on recent size optimization methodologies for standalone solar and wind hybrid renewable energy system. Energy Convers Manag 2017;143:252–74.
[13] Whitefoot JW. "Optimal co-design of microgrids and electric vehicles: synergies, simplifications and the effects of uncertainty," PhD thesis. Ann Arbor: University of Michigan; 2012.
[14] Cardoso G, Brouhard T, DeForest N, Wang D, Heleno M, Kotzur L. Battery aging in multi-energy microgrid design using mixed integer linear programming. Appl Energy 2018;231:1059–69.
[15] Costa A, Fichera A. A mixed-integer linear programming (MILP) model for the evaluation of CHP system in the context of hospital structures. Appl Therm Eng 2014;71(2):921–9.
[16] Brunetto C, Tina G. Optimal hydrogen storage sizing for wind power plants in day ahead electricity market. IET Renew Power Gener 2007;1(4):220–6.
[17] Sadeghzadeh SM, Ansarian M. Distributed generation and renewable planning with a linear programming model. In: Proceedings of the 2006 IEEE international power and energy conference. Malaysia: Putra Jaya; 2006. p. 48–53. 28–29 Nov. 2006.
[18] Han Y, Young P, Zimmerle D. Optimal selection of generators in a microgrid for fuel usage minimization. In: Proceedings of the 2013 IEEE power & energy society general meeting; 2013. p. 1–5. 21–25 Jul..
[19] Vafaei M, Kazerani M. Optimal unit-sizing of a wind-hydrogen-diesel microgrid system for a remote community. In: Proceedings of the 2011 IEEE trondheim powertech; 2011. p. 1–7. 19–23 Jun..
[20] Logenthiran T, Srinivasan D, Khambadkone AM, Raj TS. Optimal sizing of an islanded microgrid using evolutionary strategy. In: Proceedings of the 2010 IEEE 11th international conference on probabilistic methods applied to power systems; 2010. p. 12–17. 14–17 Jun..
[21] Mohammadi H, Mohammadi M. Optimization of the micro combined heat and power systems considering objective functions, components and operation strategies by an integrated approach. Energy Convers Manag 2020;208:112610.
[22] Maleki A, Askarzadeh A. Comparative study of artificial intelligence techniques for sizing of a hydrogen-based stand-alone photovoltaic/wind hybrid system. Int J Hydrog Energy 2014;39(19):9973–84.
[23] Khan B, Singh P. Selecting a meta-heuristic technique for smart micro-grid optimization problem: a comprehensive analysis. IEEE Access 2017;5:13951–77.
[24] Maleki A, Pourfayaz F. Optimal sizing of autonomous hybrid photovoltaic/wind/battery power system with LPSP technology by using evolutionary algorithms. Sol Energy 2015;115:471–83.
[25] Ramli MAM, Bouchekara HREH, Alghamdi AS. Optimal sizing of PV/wind/diesel hybrid microgrid system using multi-objective self-adaptive differential evolution algorithm. Renew Energy 2018;121:400–11.
[26] Lian J, Zhang Y, Ma C, Yang Y, Chaima E. A review on recent sizing methodologies of hybrid renewable energy systems. Energy Convers Manag 2019;199:112027.
[27] Kennedy J, Eberhart RC. Particle swarm optimization. In: Proceedings of the 1995 IEEE international conference on neural networks, 4; 1995. p. 1942–8. 27 Nov.–1 Dec..
[28] Goldberg DE, Holland JH. Genetic algorithms and machine learning. Mach Learn 1988;3:95–9.
[29] Kao YT, Zahara E. A hybrid genetic algorithm and particle swarm optimization for multimodal functions. Appl Soft Comput J 2008;8(2):849–57.
[30] Geem ZW, Kim JH, Loganathan GV. A new heuristic optimization algorithm: harmony search. Simulation 2001;76(2):60–8.
[31] Van Laarhoven PJM, Aarts EHL. Simulated annealing. In: Simulated annealing: theory and applications. Springer; 1987. p. 7–15.
[32] D. Karaboga, 2005. An idea based on honey bee swarm for numerical optimization. Technical Report-TR06, Erciyes University, Engineering Faculty, Computer Engineering Department.
[33] Dorigo M, Birattari M, Stutzle T. Ant colony optimization. IEEE Comput Intell Mag 2006;1(4):28–39.
[34] Mirjalili S. The ant lion optimizer. Adv Eng Softw 2015;83:80–98.
[35] Hakimi SM, Moghaddas-Tafreshi SM. Optimal sizing of a stand-alone hybrid power system via particle swarm optimization for Kahnouj area in south-east of Iran. Renew Energy 2009;34(7):1855–62.
[36] Li B, Roche R, Paire D, Miraoui A. Sizing of a stand-alone microgrid considering electric power, cooling/heating, hydrogen loads and hydrogen storage degradation. Appl Energy Nov. 2017;205:1244–59.
[37] Askarzadeh A. A discrete chaotic harmony search-based simulated annealing algorithm for optimum design of PV/wind hybrid system. Sol Energy 2013;97:93–101.
[38] Fetanat A, Khorasaninejad E. Size optimization for hybrid photovoltaic-wind energy system using ant colony optimization for continuous domains based integer programming. Appl Soft Comput J 2015;31:196–209.
[39] Maleki A, Askarzadeh A. Artificial bee swarm optimization for optimum sizing of a stand-alone PV/WT/FC hybrid system considering LPSP concept. Sol Energy 2014;107:227–35.
[40] Askarzadeh A, dos Santos Coelho L. A novel framework for optimization of a grid independent hybrid renewable energy system: a case study of Iran. Sol Energy 2015;112:383–96.

[41] Mohseni S, Brent AC, Burmester D. A sustainable energy investment planning model based on the micro-grid concept using recent metaheuristic optimization algorithms. In: Proceedings of the 2019 IEEE congress on evolutionary computation (CEC); 2019. p. 219–26. 10–13 Jun..

[42] Mahmoud TS, Ahmed BS, Hassan MY. The role of intelligent generation control algorithms in optimizing battery energy storage systems size in microgrids: a case study from Western Australia. Energy Convers Manag 2019;196:1335–52.

[43] El-bidari KS, Nguyen HD, Jayasinghe SDG, Mahmoud TS, Penesis I. A hybrid energy management and battery size optimization for standalone microgrids: A case study for Flinders Island, Australia. Energy Convers Manag 2018;175:192–212.

[44] Mohseni S, Brent A, Burmester D, Chatterjee A. Optimal sizing of an islanded micro–grid using meta-heuristic optimization algorithms considering demand-side management. In: Proceedings of the 2018 Australasian universities power engineering conference (AUPEC); 2018. p. 1–6. 27–30 Nov..

[45] Mohseni S, Brent AC, Burmester D. Power quality considerations in the planning phase of stand-alone wind-powered micro-grids. In: Proceedings of the 2020 19th international conference on harmonics and quality of power (ICHQP); 2020. p. 1–6. 6–7 Jul..

[46] Bornapour M, Hemmati R, Pourbehzadi M, Dastranj A, Niknam T. Probabilistic optimal coordinated planning of molten carbonate fuel cell-CHP and renewable energy sources in microgrids considering hydrogen storage with point estimate method. Energy Convers Manag 2020;206:112495.

[47] Zhang W, Maleki A, Rosen MA, Liu J. Sizing a stand-alone solar-wind-hydrogen energy system using weather forecasting and a hybrid search optimization algorithm. Energy Convers Manag 2019;180:609–21.

[48] Xu C, Ke Y, Li Y, Chu H, Wu Y. Data-driven configuration optimization of an off-grid wind/PV/hydrogen system based on modified NSGA-II and CRITIC-TOPSIS. Energy Convers Manag 2020;215:112892.

[49] Kaabeche A, Bakelli Y. Renewable hybrid system size optimization considering various electrochemical energy storage technologies. Energy Convers Manag 2019;193:162–75.

[50] Das M, Singh MAK, Biswas A. Techno-economic optimization of an off-grid hybrid renewable energy system using metaheuristic optimization approaches – Case of a radio transmitter station in India. Energy Convers Manag 2019;185:339–52.

[51] Bukar AL, Tan CW, Yiew LK, Ayop R, Tan W-S. A rule-based energy management scheme for long-term optimal capacity planning of grid-independent microgrid optimized by multi-objective grasshopper optimization algorithm. Energy Convers Manag 2020;221:113161.

[52] Singh S, Singh M, Kaushik SC. Feasibility study of an islanded microgrid in rural area consisting of PV, wind, biomass and battery energy storage system. Energy Convers Manag 2016;128:178–90.

[53] Mohseni S, Brent AC, Burmester D. A demand response-centred approach to the long-term equipment capacity planning of grid-independent micro-grids optimized by the moth-flame optimization algorithm. Energy Convers Manag 2019;200:112105.

[54] Mohseni S, Brent AC. Economic viability assessment of sustainable hydrogen production, storage, and utilisation technologies integrated into on- and off-grid micro-grids: A performance comparison of different meta-heuristics. Int J Hydrog Energy 2020;45(59):34412–36.

[55] Mohseni S, Brent AC, Burmester D. A comparison of metaheuristics for the optimal capacity planning of an isolated, battery-less, hydrogen-based micro-grid. Appl Energy 2020;259:114224.

[56] Mirjalili S. Moth-flame optimization algorithm: A novel nature-inspired heuristic paradigm. Knowl Based Syst 2015;89:228–49.

[57] Eriksson ELV, Gray EM. Optimization and integration of hybrid renewable energy hydrogen fuel cell energy systems – a critical review. Appl Energy 2017;202:348–64.

[58] Pecenak ZK, Stadler M, Fahy K. Efficient multi-year economic energy planning in microgrids. Appl Energy 2019;255:113771.

[59] HOMER Energy HOMER (Hybrid optimization models for energy resources) [Computer software]. Boulder, CO; 2020. https://www.homerenergy.com/. [Accessed: 11-Nov.-2020].

[60] Natural Resources CAMNET Energy Technology RETScreen [Computer software]; 2020. https://www.nrcan.gc.ca/maps-tools-publications/tools/data-analysis-software-modelling/retscreen/7465/. [Accessed: 11-Nov.-2020].

[61] Whitefoot JW, Mechtenberg AR, Peters DL, Papalambros PY. Optimal component sizing and forward-looking dispatch of an electrical microgrid for energy storage planning. In: Proceedings of the ASME 2011 international design engineering technical conferences and computers and information in engineering conference; 2011. p. 341–50. 28–31 Aug..

[62] HOMER Energy. HOMER Pro (Hybrid optimization models for energy resources pro) [Computer software]. Boulder, CO; 2020. https://www.homerenergy.com/. [Accessed: 11-Nov.-2020].

[63] National Renewable Energy Lab and University of Massachusetts Amherst Hybrid2 [Computer software; 2020. https://www.umass.edu/windenergy/research/topics/tools/software/hybrid2/. [Accessed: 11-Nov.-2020].

[64] National Renewable Energy Lab SAM (System advisor model) [Computer software]; 2020. [Accessed: 11-Nov.-2020].

[65] XENDEE [Computer software]. https://xendee.com/ [Accessed: 11-Nov.- 2020].

[66] National Renewable Energy Lab REopt [Computer software]; 2020. [Accessed: 11-Nov.-2020].

[67] Grid Integration Group, Berkeley Lab DER-CAM (Distributed energy resources customer adoption model) [Computer software]; 2020. https://gridintegration.lbl.gov/der-cam/. [Accessed: 11-Nov.-2020].

[68] Chawla M, Duhan M. Levy flights in metaheuristics optimization algorithms – a review. Appl Artif Intell 2018;32:802–21.

[69] Deotti LMP, Pereira JLR, da Silva Júnior IC. Parameter extraction of photovoltaic models using an enhanced Lévy flight bat algorithm. Energy Convers Manag 2020;221:113114.

[70] Li Z, Zhou Y, Zhang S, Song J. Lévy-flight moth-flame algorithm for function optimization and engineering design problems. Math Probl Eng 2016;2016:1423930.

[71] Türkay BE, Telli AY. Economic analysis of standalone and grid connected hybrid energy systems. Renew Energy 2011;36(7):1931–43.

[72] HOMER Energy Salvage Value. [Online]; 2021. Available: https://www.homerenergy.com/products/pro/docs/latest/salvage_value.html [Accessed: 12-Jan.-].

[73] Brigo D, Mercurio F. Interest rate models-theory and practice: with smile, inflation and credit. Springer Science & Business Media; 2007.

[74] Ofry E, Braunstein A. The loss of power supply probability as a technique for designing stand-alone solar electrical (Photovoltaic) systems. IEEE Power Eng Rev 1983;PER-3(5):34–5.

[75] Zhang Y, Lundblad A, Campana PE, Benavente F, Yan J. Battery sizing and rule-based operation of grid-connected photovoltaic-battery system: a case study in Sweden. Energy Convers Manag 2017;133:249–63.

[76] Pimm AJ, Palczewski J, Morris R, Cockerill TT, Taylor PG. Community energy storage: a case study in the UK using a linear programming method. Energy Convers Manag 2020;205:112388.

[77] Clean Energy Reviews Lead-acid vs lithium-ion batteries; 2020. [Online]. Available: https://www.cleanenergyreviews.info/blog/simpliphi-pylontech-narada-bae-lead-acid-battery [Accessed: 11-Nov.-].

[78] HOMER Energy Modified kinetik battery model; 2020. [Online]. Available: https://www.homerenergy.com/products/grid/docs/latest/modified_kinetic_battery_model.html/ [Accessed: 11-Nov.-2020].

[79] Lee Y-L, Tjhung T. Rainflow cycle counting techniques. In: Metal fatigue analysis handbook; 2012. p. 89–114.

[80] Y. Shi, B. Xu, Y. Tan, and B. Zhang, “A convex cycle-based degradation model for battery energy storage planning and operation,” *arXiv preprint*, arXiv:1703.07968v2, 2017.

[81] Reynolds AM. Current status and future directions of Lévy walk research. Biol Open 2018;7(1).

[82] Mohseni S, Brent AC, Burmester D. Community resilience-oriented optimal micro–grid capacity expansion planning: the case of totarabank eco-village, New Zealand. Energies 2020;13(15):3970.

[83] Totarabank – Sustainable Rural Living. https://totarabank.weebly.com/ [Accessed: 11-Nov.- 2020].

[84] Sun SI, Smith BD, Wills RGA, Crossland AF. Effects of time resolution on finances and self-consumption when modeling domestic PV-battery systems. Energy Reports 2020;6:157–65.

[85] Los Alamos National Laboratory DC microgrids scoping study–estimate of technical and economic benefits; Mar. 2015. Available: https://www.energy.gov/sites/prod/files/2015/03/f20/DC_Microgrid_Scoping_Study_LosAlamos-Mar2015.pdf [Accessed: 11-Nov.-2020].

[86] Trading Economics New Zealand – real interest rate; 2020. [Online]. Available: https://tradingeconomics.com/new-zealand/real-interest-rate-percent-wb-data.html/ [Retrieved: 5-Aug.-].

[87] Patel MR. Wind and solar power systems: design, analysis, and operation. CRC Press; 2005.

[88] CliFlo New Zealand’s national climate database; 2020. [Online]. Available: http://cliflo.niwa.co.nz/ [Retrieved: 12-Oct.-].

[89] The Electricity Market Information The New Zealand electricity authority’s wholesale database; 2020. [Online]. Available: https://www.emi.ea.govt.nz/Wholesale/Reports/ [Retrieved: 12-Oct.-].

[90] B. Anderson, D. Eyers, R. Ford, D. G. Ocampo, R. Peniamina, J. Stephenson, K. Suomalainen, L. Wilcocks, and M. Jack. *New Zealand GREEN grid household electricity demand study 2014-2018*. Colchester, Essex: UK Data Service. http://dx.doi.org/10.5255/UKDA-SN-853334.

[91] Canadian Solar Inc., “KuMax – high-efficiency poly module” Oct. 2019, PV Module Product Datasheet V5.6_AU. [Online]. Available: https://www.canadiansolar.com/test-au/wp-content/uploads/sites/2/2020/04/Canadian_Solar-Datasheet-KuDymond_CS3U-MS-AG_v5.6_AU.pdf [Accessed: 11-Nov.-2020].

[92] AWS HC Wind Turbine – Performance Series. [Online]. Available: https://80349778-823f-498f-9402-994883b1a929.filesusr.com/ugd/3830e3_1e1e44ed6ca14fa29155b9c81feaaa81.pdf [Accessed: 11-Nov.- 2020].

[93] Selectronic – SP PRO AU Series. [Online]. Available: http://download.selectronic.com.au/brochure/BR0002_10%20SP%20PRO%20Data%20Sheet%20LR.pdf [Accessed: 11-Nov.- 2020].

[94] Mohseni S, Brent AC, Kelly S. A hierarchical, market-based, non-cooperative game-theoretic approach to projecting flexible demand-side resources: Towards more realistic demand response-integrated, long-term energy planning models. In: Proceedings of the 2020 17th international conference on the European energy market (EEM); 2020. p. 1–6. 16–18 Sep..

[95] Mohseni S, Brent AC, Burmester D, Chatterjee A. Stochastic optimal sizing of micro-grids using the moth-flame optimization algorithm. In: Proceedings of the 2019 IEEE power & energy society general meeting (PESGM); 2019. p. 1–5. 4–8 Aug..

[96] Graham P. GenCost 2019-20: preliminary results for stakeholder review; 2019. [Online]. Available: https://www.aemo.com.au/-/media/Files/Electricity/NEM/Planning_and_Forecasting/Inputs-Assumptions-Methodologies/2019/CSIRO-GenCost2019-20_DraftforReview.pdf/ [Accessed: 11-Nov.-2020].

[97] HOMER Energy How HOMER calculates the PV array power output; 2020. [Online]. Available: https://www.homerenergy.com/products/pro/docs/latest/how_homer_calculates_the_pv_array_power_output.html/ [Accessed: 11-Nov.-2020].

[98] HOMER Energy How HOMER calculates wind turbine power output; 2020. [Online]. Available: https://www.homerenergy.com/products/pro/docs/latest/how_homer_calculates_wind_turbine_power_output.html/ [Accessed: 11-Nov.-].
[99] HOMER Energy Welcome to HOMER; 2020. [Online]. Available: https://www.homerenergy.com/products/pro/docs/latest/index.html/ [Accessed: 11-Nov.-2020].
[100] Ma T, Yang H, Lu L. A feasibility study of a stand-alone hybrid solar–wind–battery system for a remote island. Appl Energy 2014;121:149–58.
[101] HOMER Energy Battery Bank Autonomy; 2020. [Online]. Available: https://www.homerenergy.com/products/pro/docs/latest/battery_bank_autonomy.html/ [Accessed: 11-Nov.-2020].
[102] New Zealand's Ministry of Business Innovation & employment. *Quarterly survey of domestic electricity prices – nominal indicators on 15 August 2020*; Aug. 2020. Available: https://www.mbie.govt.nz/assets/Uploads/qsdep-report-15aug2020.pdf .
[103] International Renewable Energy Agency (IRENA) The power to change: solar and wind cost reduction potential to 2025; Jun. 2016. Available: https://www.irena.org/-/media/Files/IRENA/Agency/Publication/2016/IRENA_Power_to_Change_2016.pdf .
[104] Lin SAY. The modified internal rate of return and investment criterion. Eng Econ 1976;21(4):237–47.
[105] Ross S. Why is the modified internal rate of return (MIRR) preferable to the regular internal rate of return?; 2020. [Online]. Available: https://www.investopedia.com/ask/answers/061515/why-modified-internal-rate-return-mirr-preferable-regular-internal-rate-return.asp [Accessed: 11-Nov.-].
[106] Whitman DL, Terry RE. Fundamentals of engineering economics and decision analysis. Synth Lect Eng 2012;7(1):1–219.
[107] Johansson S-E. Income taxes and investment decisions. Swed J Econ 1969;71(2):104–10.
[108] Fioriti D, Pintus S, Lutzemberger G, Poli D. Economic multi-objective approach to design off-grid microgrids: a support for business decision making. Renew Energy 2020;159:693–704 https://doi.org/. doi:10.1016/j.renene.2020.05.154.
[109] Chen J. Profitability index [Online]; 2020. Available: https://www.investopedia.com/terms/p/profitability.asp [Accessed: 11-Nov.-].